Journal of Thermal Science Vol.30, No.2 (2021) 363−393

https://doi.org/10.1007/s11630-021-1403-x **Article ID: 1003-2169(2021)02-0363-31**

Forced Convection Heat Transfer in Porous Structure: Effect of Morphology on Pressure Drop and Heat Transfer Coefficient

ZHAO Jiafei, SUN Mingrui, ZHANG Lunxiang, HU Chengzhi, TANG Dawei, YANG Lei*, SONG Yongchen

Key Laboratory of Ocean Energy Utilization and Energy Conservation of Ministry of Education, Dalian University of Technology, Dalian 116023, China

Abstract: A light-weight structure with sufficient mechanical strength and heat transfer performance is increasingly required for some thermal management issues. The porous structure with the skeleton supporting the ambient stress and the pores holding the flowing fluid is considered very promising, attracting significant scientific and industrial interest over the past few decades. However, due to complicated morphology of the porous matrices and thereby various performance of the pressure drop and heat transfer coefficients (HTC), the comprehensive comparison and evaluation between different structures are largely unclear. In this work, recent researches on the efforts of forced convection heat transfer in light-weight porous structure are reviewed; special interest is placed in the open-cell foam, lattice-frame, structured packed bed, and wire-woven structures. Their experimental apparatus, morphological of the porous structures, effect of morphology on pressure drop and HTC, and further applications are discussed. The new method which measure morphology accurately should be paid more attention to develop more accuracy correlation. Also, the most research focused on low Reynolds number and existing structure, while very few researchers investigated the property of forced convection heat transfer in high velocity region and developed new porous structure.

Keywords: forced convection, heat transfer, heat transfer coefficient, pressure drop, morphological characteristics, porous structure

1. Introduction

Heat transfer enhancement has long been crucial for energy saving, equipment safety, and production improvement, and others. Many heat transfer devices have been developed. However, a number of thermal management issues have become evident in various fields, for example in aero-engine thermal management [1, 2], high power electron device cooling [3], and nuclear reactor cooling [4], and others [5, 6]. It has become clear that more effective compact heat transfer devices with smaller volumes are needed for such applications. Porous structures with large specific surface areas, tortuous passages and porosity [7, 8], as well as attractive mechanical properties [9, 10] is suitable to face those regard. The use of such structures to design heat transfer devices is therefore a promising avenue for addressing thermal management issues.

Received: Apr 9, 2020 AE: JIA Li Corresponding author: YANG Lei E-mail: leiyang@dlut.edu.cn

Nomenclature

A	constant
a	constant
b	constant
C	inertia coefficient/m^{-1}
c	specific heat capacity/$J \cdot kg^{-1} \cdot K^{-1}$
c_p	specific heat capacity at constant pressure/$J \cdot kg^{-1} \cdot K^{-1}$
c_1	constant
c_2	constant
d	diameter/m
E_1	viscous coefficient for Eq. (39)/m^2
E_2	inertia coefficient for Eq. (39)/m^{-1}
F	Forchheimer coefficient/m^2
f	friction factor
G	constant
H	height/m
h	heat transfer coefficient/$W \cdot m^{-2} \cdot K^{-1}$
K	permeability coefficient/m^2
k	thermal conductive/$W \cdot m^{-1} \cdot K^{-1}$
l	length/m
l'	addition length/m
Nu	Nusselt number
n	constant
PPC	pores per centimeter
PPI	pores per inch
Pr	Prandtl number
Re	Reynolds number
S_{cell}	unit cell length/m
$S_{v\text{-}g}$	geometric specific area/$m^2 \cdot m^{-3}$
S_v	specific surface area/$m^2 \cdot m^{-3}$
T	temperature/K
u	velocity/$m \cdot s^{-1}$
V	volume/m^3

Greek Symbols

α	constant
β	constant
ε	porosity
μ	dynamic velocity/Pa·s
χ	tortuosity
ρ	density/$kg \cdot m^{-1}$

Subscripts

c	cell
D	Darcy
f	foam of fluid
h	hydraulic
i	inner
o	open or outlet
p	pore or particle
s	solid or strut
t	total
v	volume
w	window

Several investigations have focused on forced convection heat transfer through porous structures, showing that such structures are able to enhance heat transfer. However, these are subject to large pressure drops in turbulence regions, with high Reynolds numbers. In order to design a compact heat transfer device, it is therefore necessary to develop a correlation for porous structures that would enable prediction of pressure drop and heat transfer. In recent decades, some authors have developed methods and correlations for morphological characterization and to determine pressure drop and heat transfer coefficients for a number of porous structures. However, there are no such general predictive correlations for certain random porous structures, such as open-cell foam structures, due to differences in morphological characterization, different experimental conditions and methods, and different theoretical backgrounds. It is easier to develop predictive correlations for regular porous structures (such as lattice-frame structures, structured packed beds, and wire-woven structures) than for random porous structures. However, many different structures need to be investigated for different applications of heat transfer enhancement. In addition, several reviews of heat transfer in porous media were published [11–13]. However, the focus of those reviews is media with low porosity, flowing in porous media with nanofluid, or application of porous media. We hope to figure out the key factors which affect the accuracy of predicted correlations and to give the future research interest for the industrial application of porous structure. Therefore, it is thus essential to explore the similarities and differences between these various methods and correlations by reviewing previous literature.

As briefly discussed, predictive correlations are crucial for forced convection heat transfer in porous structures; however, relevant studies remain limited. The aim of this study is two-fold: providing a basic understanding of forced convection heat transfer properties in porous media and revealing gaps in present

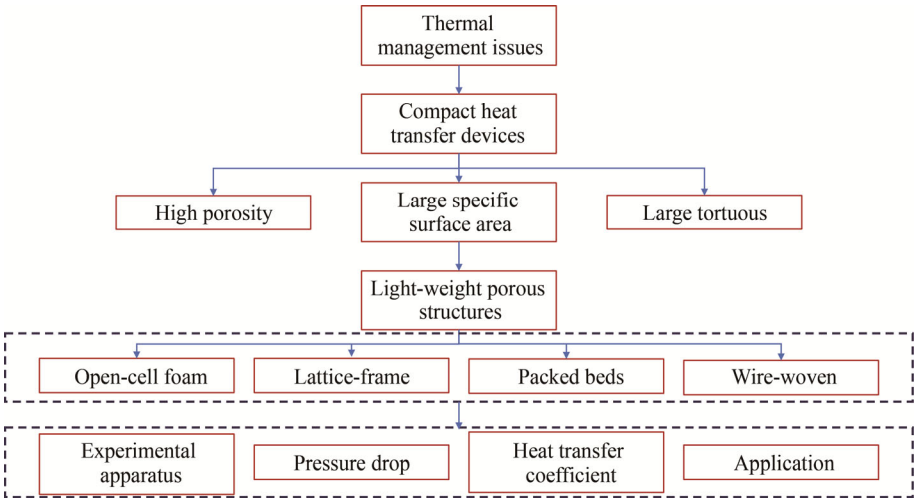

Fig. 1 The conceptual framework of present review

research. This study provides a brief review of the application of forced convection heat transfer in light-weight porous media, including open-cell foam structures, lattice-frame structures, structured packed bed structures, and wire-woven structures. This review considers experimental apparatus, the morphological characteristics of porous structures, the effect of morphology on pressure drop, HTC, and applications for heat transfer enhancement. Predictive correlations for forced convection in porous structures are compared and summarized. This review makes a significant contribution to the literature, given that few such reviews considering the effect of morphology on pressure drop and HTC for porous structure have yet been published. In addition, the conceptual framework is shown in Fig. 1.

2. Experimental Apparatus

In the case of porous structures, the loop is the basic experimental apparatus for determining pressure drop, HTC, and the properties of heat exchangers. As shown in Fig. 2, this mainly consists of an air/fluid source, heater, testing section, and data acquisition section. The electrical heater is used by many author for heating air/fluid, besides, several heating loop are used in experimental system [14–16]. The function of each loop section differs from different applications. For pressure drop measurement, the heater can be bypassed to reduce pressure loss. However, the heater is necessary to determine the HTC. The position of the heater can also vary with different experimental methods: (1) before the test section for heating fluids (transient methods), or (2) heating the test section (steady-state methods). To determine heat exchanger properties, another loop is needed to provide cooling/heating media.

Table 1 summarizes the parameters of several loops which use air and water as work medium. The air compressor and blower mostly were used to provide air. The velocity range of most loops is within 0 m/s to 16 m/s, with the velocity range of the Dukhan loop being 0.5 m/s to 35 m/s. As shown in Fig. 2, the loop can be classified as positive or negative based on the position of the air/fluid source. The air compressor is used as the air source of a positive pressure loop which given in Table 1, while the blower is used for the negative pressure loop. The positive pressure loop can provide a wider inlet pressure according to the different experimental requirements. However, there is little research specifically discussing the inlet pressure of loops. The most important element of the loop is the measuring equipment. Pressure transmitters and thermocouples are widely used for this purpose. Furthermore, an IR camera [17] and thermochromic liquid crystals [9] can be used to determine temperature distribution.

The basic components of loops are similar, and the commonly-used measuring equipment can only determine the macro characteristics of forced convection

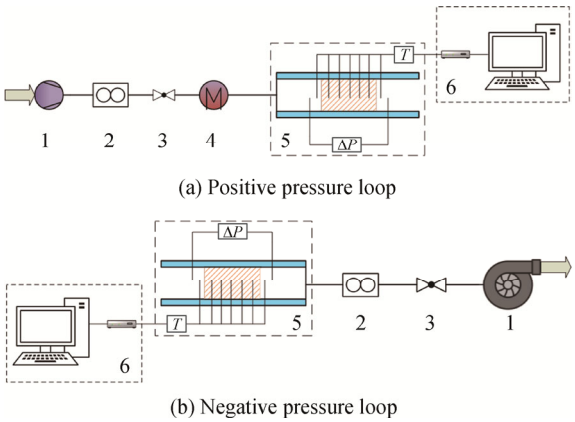

Fig. 2 Scheme of loop, (a) positive pressure loop, (b) negative pressure loop: 1. air/fluid source, 2. flowmeter, 3.heater, 4. control valve, 5. testing section, 6. data acquisition

Table 1 Summary of experimental apparatus parameters and applications

Authors	media	Velocity/m·s^{-1}	Pressure/kPa	Applications	Air source
Mancin et al. [18–21]	air	2.00 to 5.00	700	HTC Pressure drop	Air compressor system
Dirtrich et al. [22, 23]	air	0.50 to 9.00	–	HTC Pressure drop	Blower
Wallenstein et al. [24]	air	0.60 to 3.00	–	HTC	Not mentioned
Moreira et al. [25, 26]	air or water	0.00 to 18.50 (air) 0.00 to 0.33 (water)	–	Permeability	Air compressor system pump
Giani et al. [27]	air	1.00 to 16.00	–	Pressure drop	–
Xia et al. [28]	air	2.00 to 9.00	–	HTC	Air compressor system
Lacroix et al. [29]	air	0.00 to 5.00	–	Pressure drop	Not mentioned
Dixit et al. [30]	air	0.8 to 5.50	Negative	Pressure drop HTC	Blower
Yan et al. [31]	air	2.87 to 12.52	–	Pressure drop	Blower
Kurian et al. [32]	air-water	0.50 to 3.00	–	Heat exchanger	Blower
Nawaz et al. [33]	air-water	0.30 to 7.00	–	Heat exchanger	Blower (cycle)
T'joen et al. [34]	air-water	0.70 to 7.40	–	Heat exchange	–
Chen et al. [35]	air-water	0.50 to 12.00	1200	Heat exchanger	Air compressor system
Fuller et al. [7]	air	0.00 to 16.00	–	HTC	Blower
Madani et al. [36]	water	0.00 to 0.20	–	Pressure drop	Pump
Garrido et al. [37]	air	0.00 to 15.00	–	Pressure drop	–
Son et al. [38]	air	0.05 to 1.00	Negative	HTC pressure drop	Blower
Dukhan et al. [39]	air	0.5 to 35	Negative	Permeability	Blower

heat transfer in porous structures. Measurement at pore scale is difficult and few authors have investigated this in detail. More effective measuring equipment is needed for determination of heat transfer properties at pore scale.

3. Morphological Characterization of Porous Structures

The pressure drop and heat transfer performance of porous structures greatly depend on their morphological characterization; this therefore provides a basis for applications of porous structures. Accurate morphological characterization of such structures is important for measurement of pressure drop and HTC.

3.1 Morphological characterization of open-cell foam structures

The open-cell foam structures manufactured by different method have different morphological characteristics. As shown in Fig. 3, there are different types of open-cell foam structures. The dimension and form of skeletons are very different among four types of open-cell foam structure. In addition, the pores of foam manufactured by using powdered metal are more closed than other three foams. Therefore, the open-cell foam structure discussed at present work did not include the foam manufactured by using powdered metal. Banhart et al. [40] classified production methods of metallic foam

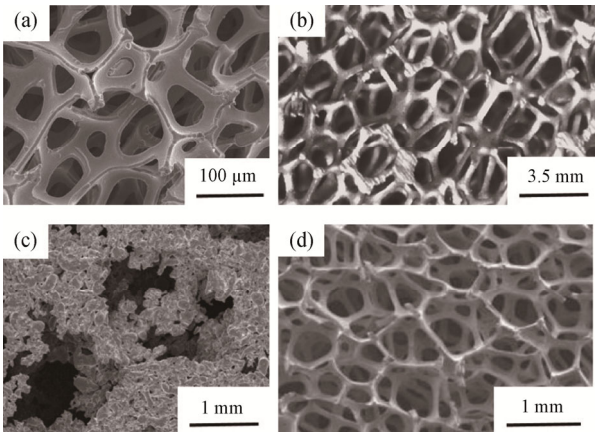

Fig. 3 (a) Using vapor technology to produce "INCOFOAM" [42]; (b) using liquid metal to produce "Duocel" aluminum foam [43]; (c) using powdered metal to produce inconel 600 foam [44]; (d) using metal ions to produce nickel foam [45]

structures into metal vapor, liquid metal, powdered metal, and metal ions, according to the state of the metal. Deng et al. [41] reviewed production methods of ceramic foams for fabricating porous ceramics, classifying these into direct foaming, three-dimensional printing, and molten salt methods.

Several geometrical characters are used to describe the open-cell foam structure: ε (porosity), PPI (pores per

inch), d_s (strut diameter), d_w (window diameter), d_c (cell diameter), S_v (specific surface area), χ (geometric tortuosity), and others. The manufacturer generally only provides ε and sometimes PPI; other geometry characters therefore need to be measured or calculated. In the literature, ε, d_s, d_w, d_c, and S_v are often used to develop the correlation between pressure drop and HTC for open-cell foam structures. In the following section, methods for determining ε, d_s, d_w, d_c and S_v are reviewed.

3.1.1 Porosity

ε is defined as the fluid storage capacity of porous media [46]. Normally, ε of open-cell foam can be determined using Eq. (1). Here, V is the volume of foam; V_s is the volume of the solid skeleton, and ρ_f is the density of foam, i.e., the specific value of the mass of the foam sample and apparent volume of the foam sample. ρ_s is the density of the solid. However, as shown in Fig. 4, the strut of most open-cell foams is hollow due to the production methods-replication technique [47]. Inayat et al. [48] summarized porosities as: ε_o open porosity, ε_s strut porosity, ε_i total porosity, and ε_n normal porosity, which is given by the manufacturer.

$$\varepsilon_t = 1 - \frac{V_s}{V} = 1 - \frac{\rho_f}{\rho_s} \tag{1}$$

In the literature, many different ways of measuring ε_i, ε_o, and ε_s are presented, such as magnetic resonance imaging (MRI), Scanning Electron Microscopy (SEM), and mercury porosimetry. Crosse et al. [49] used MRI to determine ε_i and ε_o by counting solid voxels in unfilled data and counting solid voxels in filled data respectively. ε_s can be calculated using Eq. (2):

$$\varepsilon_s = \varepsilon_t - \varepsilon_o \tag{2}$$

Fuller et al. [7] used SEM images to determine the average ligament inner d_i and outer diameter d_o. ε_o can be determined using Eq. (3):

$$\varepsilon_o = 1 - \frac{\rho_f}{\rho_s}\left(\frac{1}{1-\left(d_i / d_0\right)^2}\right) \tag{3}$$

Some authors [37, 50] have used mercury porosimetry to measure ε_i and ε_o. This involves first using mercury intrusion in large pores and obtaining V_o (volume of open pores) at atmospheric pressure. Mercury is then used to fill every pore of open-cell foam at high pressure and obtain V_s. Finally, ε_i, ε_o, and ε_s can be determined. However, since mercury cannot be used to fill every pore, this method is not suitable for every open-cell foam. Therefore, the approach which measures porosity more accurately should be paid much more attention.

ε_o is hard to measure in all samples and is therefore neglected by many authors. ε_i is instead used to develop the correlation between pressure drop and HTC. Inayat et al. [48] investigated differences in pressure drop prediction with ε_i and ε_o. The authors found that the small difference between ε_i and ε_o can lead to a significant influence on the prediction of pressure drop. To determine heat transfer progress, the authors use the correlation determined by Xia [28] to predict Nu_v using five ε levels, with a difference of only 0.03 between these. As shown in Fig. 5, this small difference can significantly impact Nu_v. Therefore, ε_s must be accurately determined, in particular when open-cell foam is used under high velocity conditions. For open-cell foam in which ε_s is 0, ε_s is equal and can be determined using Eq. (1) directly. In the other hand, the existence of ε_s influences the effective thermal conductivity of open-cell foam significantly, and then the overall heat transfer performance decreases. Therefore, the new method which manufactured open-cell foam without hollow skeletons should be developed such as additive manufacturing.

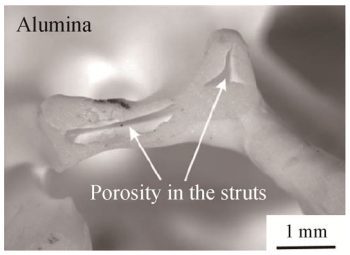

Fig. 4 Hollow strut of open-cell foam [8]

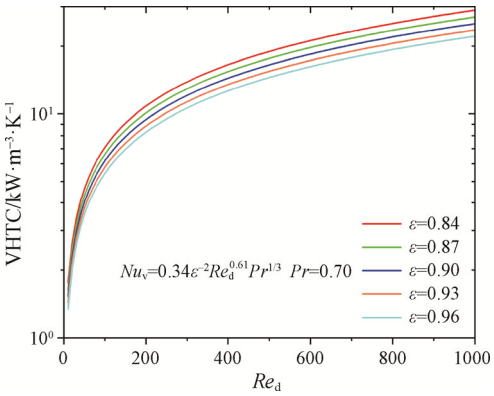

Fig. 5 Prediction of Nu_v with five ε which have the difference only 0.03 by using correlation of Xia [28]

3.1.2 Pore diameter

Pore diameter had been extensively defined [20, 51] and measured [23] over past decades. However, it is interpreted differently by different authors, with definitions used including average diameter with an area the same as that of the tetrakaidecahedral window [52], or average diameter with a volume the same as that of a sphere [53], or 25.4 mm/PPI [20, 21]. To address this problem of unclear definition, Inayat et al. [48] defined

four characteristic pore diameters: d_w (average window diameter), d_s (strut diameter), d_c (average cell diameter), and D_p (average value of sum, d_s+d_w). Additionally, some authors [23, 54, 55] use hydraulic diameter d_h to develop a correlation, while others use d_p (equivalent particle diameter) as a characteristic length scale. Several authors [56, 57] also use $\sqrt{K}$ due to the different definition and measurement of morphological characteristics, where K is the permeability coefficient. However, the values of K obtained experimentally are not accurate, and thus using K as a length scale has limitations.

It is easy to measure the values of d_s and d_w using SEM, light microscopy images, and 3D scanned images [37, 58, 59], but these techniques may be less effective for determining d_p and d_c. Furthermore, d_h cannot be measured using such equipment. Correlations have therefore been developed to determine d_p, d_c, and d_h.

In the literature [27, 29], equivalent particle diameter d_p has been calculated using Eqs. (4) and (5), which were developed using the cubic cell model and pentagonal dodecahedron geometry, respectively. Neither correlation can be applied to every sample due to changes in pore diameter with manufacturing processes [60]; errors in these correlations can lead to significant errors in results.

$$d_p = 6\left(1-\varepsilon_o\right)/S_v \tag{4}$$

$$d_p = 1.5 d_s \tag{5}$$

Eq. (6) is referenced in some studies [29, 61] for calculation of d_c. Huu et al. [62] investigated the coefficient between d_c and d_w for a ε in the range of 0.8 to 0.92. Results showed that 2.3 is a good approximation and can be used by future authors. d_h is not a morphological character of open-cell foam struts and is merely a characteristic length scale which can only be determined through correlations. Several authors [27, 54] used Eq. (7) to determine d_h, while Dietrich et al. [23] developed a simple correlation between d_h and the value of PPI (Eq. (8)).

$$d_c = 2.3 d_w \tag{6}$$

$$d_h = 4\frac{Cross\ \text{section available for flow}}{\text{wetted perimeter}} = \frac{4\varepsilon_o}{S_v} \tag{7}$$

$$d_h = 0.028(m)\,\mathrm{PPI}^{-0.721} \tag{8}$$

The above definitions and pore diameter correlations have been used by different authors as a characteristic length scale for development of predictive correlations. This is one of the reasons for the lack of a unified correlation. In addition, the concept of different diameter is shown in Table 2. Eqs. (4), (7) and (8) establish the relationship between pore diameter and d_s, ε_o, S_v, PPI, respectively. And then, the errors of d_s, ε_o, S_v and PPI will influence accuracy of pore diameter. Therefore, d_w and d_s are better choices to develop predictive correlations and used by many researcher.

3.1.3 Tortuosity

Kozeny et al. [63] defined tortuosity (χ) as the radio of effective (tortuous) path l_e to the thickness of the porous medium. It is significant for describing the morphology and transport properties of open-cell foam structures. Furthermore, the permeability and turbulence of transport in open-cell foam structures can be directly influenced by tortuosity.

Some authors have used different methods to determine tortuosity, such as ultrasonic transverse transmission methods [64], finite volume techniques [65], geometrical approaches [61, 66, 67], diffusion techniques [63, 68] and electrical resistivity methods [26]. Other authors have developed correlations to calculate tortuosity. For example, Du Plessis et al. [69] developed a model for tortuosity as a function of ε by using the cubic representative unit cell, given in Eq. (9):

$$\frac{1}{\chi} = \frac{3}{4\varepsilon_o} + \frac{\sqrt{9-8\varepsilon_o}}{2\varepsilon_o} \times \cos\left\{\frac{4\pi}{3} + \frac{1}{3}\cos^{-1}\left[\frac{8\varepsilon_o^2 - 36\varepsilon_o + 27}{\left(9-8\varepsilon_o\right)^{3/2}}\right]\right\} \tag{9}$$

Bhattacharya et al. [70] investigated whether the correlation developed by Du Plessis remains accurate in high PPI ranges, subsequently developing another correlation for determining tortuosity (Eq. (10)), which is accurate across a wide range of PPI values:

Table 2 The concept of diameter

Diameter	Concept
d_w and d_s	Measured by using SEM, light microscopy images, and 3D scanned images
D_p	average value of sum (d_s+d_w)
d_p	$d_p=6(1-\varepsilon_o)/S_v$ or $d_p=1.5d_s$
d_c	$d_c=2.3d_w$
d_h	$d_h = 4\frac{\text{Cross section available for flow}}{\text{wetted perimeter}} = \frac{4\varepsilon_o}{S_v}$ or $d_h = 0.028(m)\,\mathrm{PPI}^{-0.721}$

$$\frac{1}{\chi}=\frac{\pi}{4\varepsilon_{\mathrm{o}}}\left\{1-\left(1.18\sqrt{\frac{\left(1-\varepsilon_{\mathrm{o}}\right)}{3\pi}}\frac{1}{G}\right)^{2}\right\}=\frac{\pi}{4\varepsilon_{\mathrm{o}}}\left\{1-\left(1.18\sqrt{\frac{\left(1-\varepsilon_{\mathrm{o}}\right)}{3\pi}}\frac{1}{1-\mathrm{e}^{-\left(1-\varepsilon_{\mathrm{o}}\right)/0.04}}\right)^{2}\right\} \tag{10}$$

Inayat et al. [48] developed a correlation to determine tortuosity using a tube model, as in Eq. (11):

$$\chi=\frac{l'}{1}=1+\frac{d_{\mathrm{w}}\left(\pi d_{\mathrm{w}}l'/v\right)}{4\varepsilon_{\mathrm{o}}}=1+\frac{\mathrm{Dimensionless}\left(S_{\mathrm{v}}\right)}{4\varepsilon_{\mathrm{o}}} \tag{11}$$

Here, v is the volume of the tube model; l' is additional length; S_{v} is the dimensionless specific surface area of the open-cell foam structure.

Tortuosity can be easily determined using the above methods and correlations but the relationship between tortuosity and thermodynamic properties is not yet clear. There is a need for further model development to describe this relationship.

3.1.4 Specific surface area

The S_{v} of an open-cell foam structure is defined as the S_{v} per unit geometric volume [37]. From the correlations in Eqs. (4), (7), and (11), it is known that S_{v} is an important parameter to determine equivalent particle diameter d_{p}, average cell diameter d_{c}, hydraulic diameter d_{h}, and tortuosity χ. A large S_{v} is an advantage for many applications of open-cell foam structures, such as heat exchangers, catalyst supports, porous burners, and gas filters [50]. In addition, the accurate determination of S_{v} plays an important role on the design of heat transfer equipment.

In the literature, many methods have been used to measure S_{v} of an open-cell foam structure, such as X-ray absorption tomography [50, 71, 72], MRI [23, 49], and some novel methods. Diao et al. [73] used cyclic voltammetry and quantitative stereology to measure the S_{v} of Cu open-cell foam. However, such methods are inconvenient and expensive and not suited for engineering purposes. Therefore, the correlations that enable prediction of S_{v} are needed and some such correlations were developed in previous literature. For example, Giani et al. [27], Lacroix et al. [29], and Liu et al. [74] used the cubic cell model to develop the correlation for predicting S_{v}:

$$S_{\mathrm{v}}=\frac{4\left(1-\varepsilon_{\mathrm{o}}\right)}{d_{\mathrm{s}}} \tag{12}$$

However, the cubic model does not represent well the cell of open-cell foam structures. Gisbson et al. [75] investigated three different models (hexagonal prisms, tetrakaidecahedral, and dodecahedral), concluding that the tetrakaidecahedral model is the best suited for open-cell foam structures. Buciuman et al. [76] and Kumar et al. [77] used the tetrakaidecahedral model to develop correlations for predicting S_{v}. However, Kumar's correlation, which uses three dimensionless parameters, as shown in Eqs. (13) and (14), is too complex to use:

$$S_{\mathrm{v}}=4.82\frac{1}{D_{\mathrm{p}}}\sqrt{\left(1-\varepsilon_{\mathrm{o}}\right)} \tag{13}$$

$$S_{\mathrm{v}}=\frac{1}{\sqrt{2}L}\left[\frac{3}{2}\alpha\beta\left(2\pi-3\Omega+\frac{45}{32}\pi\alpha^{2}\left(1-\varepsilon_{\mathrm{s}}\right)\right)\right] \tag{14}$$

where α and β can be calculated by combining Eqs. (15) and (16), and Ω can calculated using Eq. (17).

$$1.6\alpha+\beta=1 \tag{15}$$

$$12\pi\alpha^{2}\beta\left(1-\varepsilon_{\mathrm{s}}\right)+\frac{32}{3}\pi\alpha^{3}\left(1-\Omega\varepsilon_{\mathrm{s}}\right)=8\sqrt{2}\left(1-\varepsilon_{\mathrm{t}}\right) \tag{16}$$

$$\Omega=\sqrt{4\pi\varepsilon_{\mathrm{s}}/\sqrt{3}} \tag{17}$$

Richardson et al. [59] investigated three different geometric models to develop the correlations given in Eqs. (18), (19), and (20) respectively and compared S_{v} values calculated using these three correlations. The authors found the values to be close to each other and selected Eq. (18) for prediction of S_{v}.

$$S_{\mathrm{v}}=\frac{4\varepsilon_{\mathrm{o}}}{d_{\mathrm{w}}} \tag{18}$$

$$S_{\mathrm{v}}=\frac{4}{d_{\mathrm{w}}} \tag{19}$$

$$S_{\mathrm{v}}=\frac{12.979\left[\left(1-\varepsilon_{\mathrm{o}}\right)^{0.5}-0.971\left(1-\varepsilon_{\mathrm{o}}\right)\right]}{d_{\mathrm{w}}} \tag{20}$$

Grosse et al. [78] developed a correlation (Eq. (21)) using the Weaire-Phelan model but this correlation did not fit experimental results well. The coefficients were therefore redefined by fitting experimental data, as shown in Eq. (22):

$$S_{\mathrm{v}}=\frac{8.21\sqrt{\left(1-\varepsilon\right)}-1.55\left(1-\varepsilon\right)}{d_{\mathrm{w}}+d_{\mathrm{s}}} \tag{21}$$

$$S_{\mathrm{v}}=\frac{4.84\sqrt{\left(1-\varepsilon_{\mathrm{o}}\right)}-2.64\left(1-\varepsilon_{\mathrm{o}}\right)}{d_{\mathrm{w}}+d_{\mathrm{s}}} \tag{22}$$

Inayat et al. [50] used the tetrakaidecahedral model to develop three correlations with different strut shapes, i.e., cylindrical, triangular, and triangular concave struts, given in Eqs. (23), (24), and (25), respectively. In other literature [48], the same authors use several correlations developed by different authors to predict S_{v} and compare with experimental data from other literature. Results showed that correlations almost always overestimate experimental data in the range of low porosity (ε_{o}< 90%). However, Eqs. (23) to (25) showed good agreement with experimental data. Due to limited availability of

experimental data from the literature, the authors did not compare theoretical with measured values.

$$S_{\text{v-cylindrical}} = 4.867\frac{\left[1-0.971\left(1-\varepsilon_{\text{o}}\right)^{0.5}\right]}{d_{\text{w}}\left(1-\varepsilon_{\text{o}}\right)^{0.5}}\left(1-\varepsilon_{\text{o}}\right) \quad (23)$$

$$S_{\text{v-triangular}} = 5.62\frac{\left[1-0.971\left(1-\varepsilon_{\text{o}}\right)^{0.5}\right]}{d_{\text{w}}\left(1-\varepsilon_{\text{o}}\right)^{0.5}}\left(1-\varepsilon_{\text{o}}\right) \quad (24)$$

$$S_{\text{v-triangular-concave}} = 6.49\frac{\left[1-0.971\left(1-\varepsilon_{\text{o}}\right)^{0.5}\right]}{d_{\text{w}}\left(1-\varepsilon_{\text{o}}\right)^{0.5}}\left(1-\varepsilon_{\text{o}}\right) \quad (25)$$

In summary, all above correlations are subject to errors in predicting S_{v} and have limited information for high porosity ranges (ε>90%). However, the correlations based on the tetrakaidecahedral model may agree well with periodic open-cell foam structures manufactured by 3D printing.

3.2 Morphological characterization of lattice-frame structures

The literature discusses different lattice-frame structures produced through various manufacturing technologies, such as brazing and assembling [79], metal wire weaving [80], investment casting [81], metal sheet folding [82, 83], and 3D printing [38]. As shown in Fig. 6, there are four lattice-frame structures (tetrahedral, pyramidal, kagome, and X-type), produced through various manufacturing methods. This section will review these four types of structures, and their ε and S_{v}.

3.2.1 Tetrahedral structure

Fig. 7 shows the details of the tetrahedral structure. Although there is little literature that provides correlations to predict ε and S_{v}, Kim et al. provide a correlation for calculating ε and S_{v} of a tetrahedral structure, as shown in Eqs. (26) and (27), respectively:

$$\varepsilon = 1-\frac{\sqrt{3}}{2}\left(\frac{d}{l}\right)^2\left(\frac{l}{H}\right) \quad (26)$$

$$S_{\text{v}} = \frac{\frac{3}{d}+2S_x l-3\frac{d^2}{4}}{HS_x l} \quad (27)$$

Eq. (26) includes three variates: diameter of ligament, length of ligament, and height of cell. According to the geometrical relationship between height and length of ligament, the two variates can be integrated into one. Son et al. [38] gave a correlation of ε with two variates, as in Eq. (28):

$$\varepsilon = 1-\frac{\sqrt{2}}{2}\left(\frac{d}{l}\right)^2+\frac{\sqrt{66}+2\sqrt{3}}{9}\left(\frac{d}{H}\right)^3 \quad (28)$$

Definitions of d, l, H, and S_x can be obtained from Fig. 7.

3.2.2 Pyramidal structure

Fig. 8 shows the details of a pyramidal structure with hollow strut. However, when the pyramidal structure is used for enhancing heat transfer, the strut must be solid due to its high thermal conductivity. There are hardly any correlations for predicting ε in relevant heat transfer literature. However, mechanics literature gives some correlations for predicting ε. St-Pierre et al. [84] developed a correlation for predicting the relative density $\bar{\rho}$ of a pyramidal structure with hollow strut. The correlation for ε can then be derived as shown in Eq. (29):

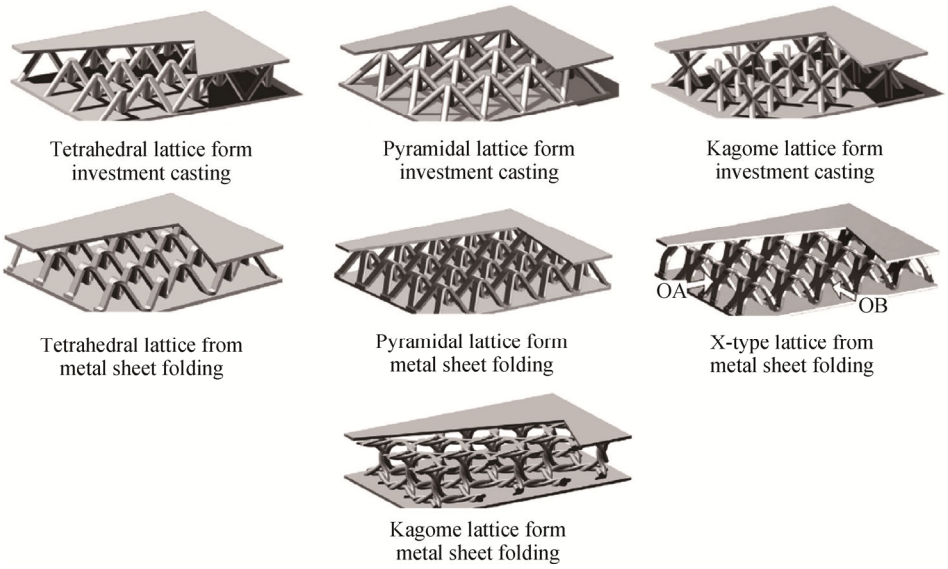

Fig. 6 Different lattice-frame structure with different manufacturing methods [31]

$$\varepsilon = 1-\overline{\rho} = 1-\frac{2\pi\left(d^2-\left(d-2t\right)^2\right)}{\left(4k+2l\cos\omega\right)^2\sin w} \tag{29}$$

Details of d, t, k, and ω can be obtained from Fig. 8. For a pyramidal structure with solid strut, t in Eq. (29) can equal $d/2$ and the correlation can be thus changed to that shown in Eq. (30). When k is equal to 0, Eq. (30) can be changed to Eq. (31), as in the correlation developed by Wei et al. [85]:

$$\varepsilon = 1-\overline{\rho} = 1-\frac{2\pi d^2}{\left(4k+2l\cos\omega\right)^2\sin w} \tag{30}$$

$$\varepsilon = 1-\overline{\rho} = 1-\frac{2\pi d^2}{\left(2l\cos\omega\right)^2\sin w} \tag{31}$$

The shape of the pyramidal structure differs in different literature, with different correlations for calculating ε of pyramidal structures [86–88]. However, there is little research that considers determination of S_v.

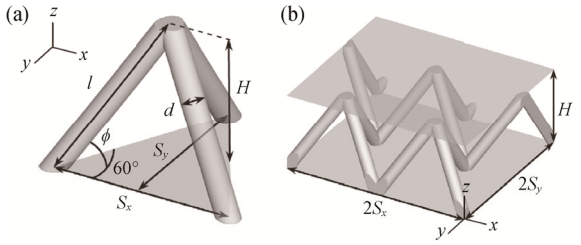

Fig. 7 Detail of tetrahedral lattice-frame structure [38]

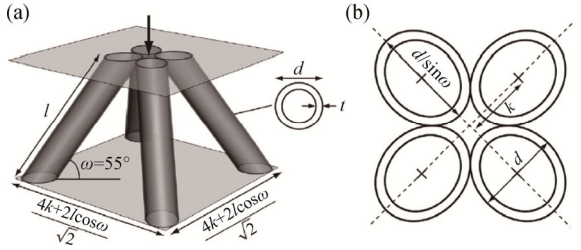

Fig. 8 Detail of pyramidal lattice-frame structure with hollow strut [84]

When using a pyramidal structure for heat transfer, the S_v is a significant characteristic and should be determined. A correlation for this purpose should therefore be developed.

3.2.3 X-type structure

No correlation for Kagome structure morphological parameters was found in available literature; however, Yan et al. [83] developed correlations for predicting ε and specific area of X-type structures, as shown in Eqs. (32) and (33), respectively:

$$\begin{aligned}\varepsilon = 1-\frac{t_1}{lwH}\Bigg[&wl_1-4\left(\frac{w-b_1}{2}+r_2\Big/\cos\frac{\beta}{2}-r_2\right)\\&\times\left(\frac{l-b_2}{2}+r_1\Big/\sin\frac{\beta}{2}-r_1\right)\\&+4\left(\cot\frac{\beta}{2}-\frac{\pi-\beta}{2}\right)r_1^2+4\left(\tan\frac{\beta}{2}-\frac{\beta}{2}\right)r_2^2\Bigg]\end{aligned} \tag{32}$$

$$\begin{aligned}S_v = \frac{2\left(1-\varepsilon\right)}{t_1}+\frac{8t_1}{lwH}\Bigg\{&\left(1\Big/\sin\frac{\beta}{2}\right)\\&\cdot\Bigg[\frac{w}{4}-w_1\Big/\left(2\cos\frac{\beta}{2}\right)+\frac{l_1}{4}\tan\frac{\beta}{2}\\&+\left(\frac{\pi-\beta}{2}-\cot\frac{\beta}{2}\right)r_1+\left(\frac{\beta}{2}-\tan\frac{\beta}{2}\right)r_2\Bigg]\Bigg\}\end{aligned} \tag{33}$$

Definitions of the following dimensions: l, w, w_1, H, t, t_1, b_1, b_2, r_1, r_2, r_3, α, and β, can be obtained from Fig. 9. l_1 can determined using Eq. (34):

$$\begin{aligned}l_1 = l\Big/\sin\frac{\alpha}{2}&+\left(2\pi-2\alpha-4\cot\frac{\alpha}{2}\right)r_3\\&+\left(\pi-\alpha-2\cot\frac{\alpha}{2}\right)t_1\end{aligned} \tag{34}$$

The morphology of lattice-frames is simpler than that of metal foams; however, there are no correlations for predicting ε and S_v of these structures. The relationship between characteristics of lattice-frames which are easily measured and those that are hard to measure should be therefore more widely investigated, and related correlations should be developed.

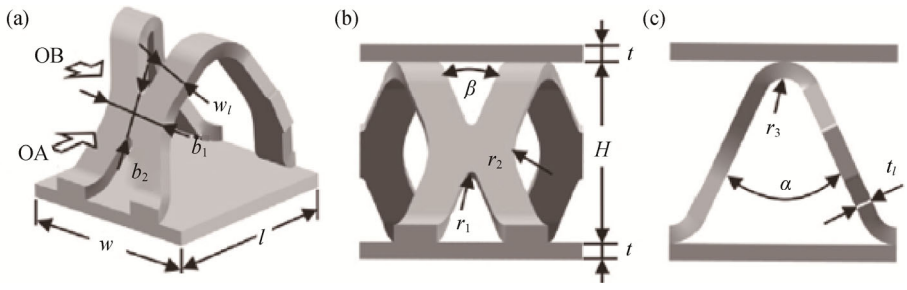

Fig. 9 Detail of x-type [83]

3.3 Morphological characterization of structured packed beds and wire-woven structures

Wire-woven metal and packed bed structures, which can serve porous media for heat transfer, can have a variety of complex structures; it is therefore difficult for a single correlation to explain their morphological characterization. However, ε, a fundamental character, can be predicted through correlations developed by some authors.

3.3.1 Packed beds

Based on packing method, packed beds can be classified as random or structured. Van Antwerpen et al. [89] reviewed descriptions of random packed beds in the literature and related correlations for predicting ε; noting that however, there are too many factors of influence to allow accurate prediction: packing mode (very loose random packing (ε: 0.46 to 0.47), loose random packing (ε: 0.40 to 0.41), poured random packing (ε: 0.375 to 0.391), close random packing (ε: 0.359 to 0.391)) [90], Wall effect [91], ratio of tube and particle diameter [92], roughness of the particle surface, particle shape and size distribution [93], the shape of the container [94], particle material density [95], and the ratio of filling height and particle diameter [96], and others. Few authors have investigated structured packed beds, but Romkes et al. [97] investigated the thermodynamic properties of composite structured packing (CSP), shown in Fig. 10. Wang et al. [98] developed a grille-sphere composite structured packed bed (GSCSPB), also shown in Fig. 10.

3.3.2 Wire-woven structure

The morphology of wire-woven metal is classified by Kang [80] as single-layered or multi-layered, depending on the process of manufacture. As shown in Fig. 11, single-layered structures include the Pyramid [99], Circular Spring Kagome (CSK) [100, 101], Hexagonal Spring Kagome (HSP) [101], Dual Wired Octet (DWO) [101, 102], Dual Wired Kagome-1 (DWK-1) [102], Dual Wired Kagome-2 (DWK-2) [101, 102], Zigzag truss [103, 104], and Three dimensional woven wire structure (3DWT) [105, 106], and others. As shown in Fig. 12, multi-layered structures include Textilecore [107], Wire-woven Bulk Kagome (WBK) [108], Struwire [109], Wire-woven Bulk Diamond (WBD) [110], Wire-woven Bulk Cross (WBC) [111, 112], and '3WEAVE' [113]. Kang [80] summarized correlations for predicting ε for the above structures, determining the following order for the ε of single-layered structures: HSK<CSK<DWK-1 = DWK-2 <DWO<Pyramid<3DWT<Zigzag. The order of ε of multi-layered structures was as follows: Textilecore<WBC<WBD< Strucwire<WBK.

The above structures all can enhance heat transfer at special condition. However, the comparison among those structures is hard to obtain by using non-dimensional number due to the different characteristic length. Field synergy is a novel concept for realizing that the flow field plays a very important role in convective heat transfer [114]. The synergy angle is an important parameter which could evaluate the overall heat transfer performance of porous structure in this theory. In

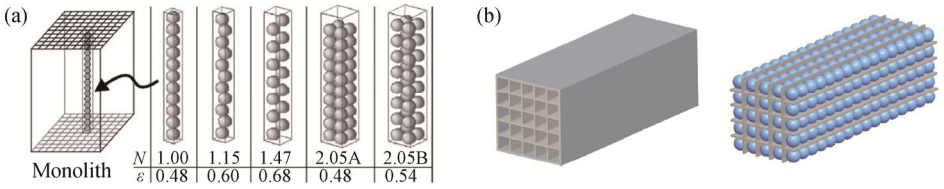

Fig. 10 Concept of (a) composite structured packing (CSP) [97]; (b) grille-sphere composite structured packed bed (GSCSPB) [98]

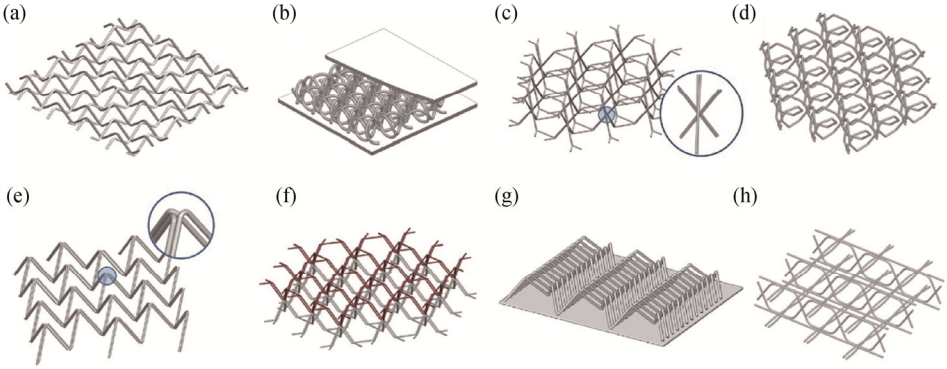

Fig. 11 Concept of single-layering: (a) Pyramid, (b) Circular Spring Kagome (CSK), (c) Hexagonal Spring Kagome (HSK), (d) Dual Wired Octet (DWO), (e) Dual Wired Kagome-1 (DWK-1), (f) Dual Wired Kagome-2 (DWK-2), (g) Zigzag truss, (h) Three dimensional woven wire structure (3DWT) [80]

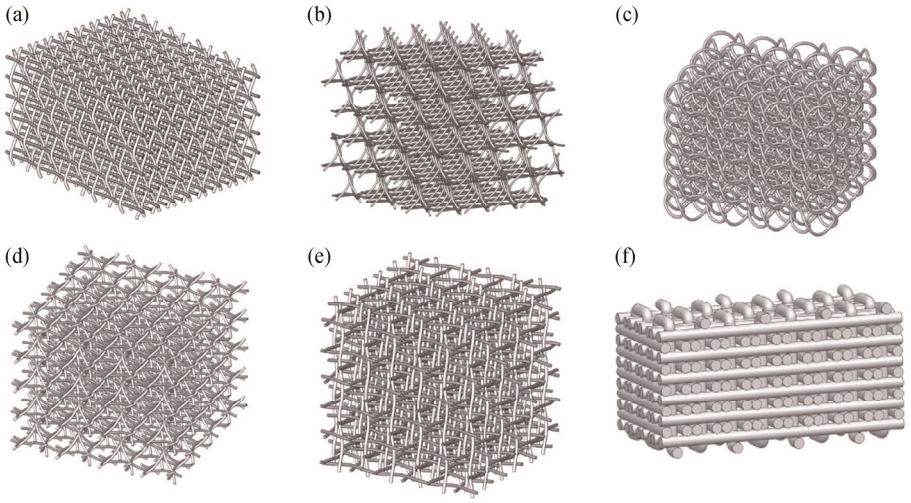

Fig. 12 Concept of multi-layering: (a) Textilecore, (b) Wire-woven Bulk Kagome (WBK), (c) Struwire, (d) Wire-woven Bulk Diamond (WBD), (e) Wire-woven Bulk Cross (WBC), (f) 3WEAVE [80]

addition, field synergy theory has been widely used in the multidisciplinary optimization of porous media [115–117]. Therefore, field synergy theory can be used to developed new porous structure which enhances heat transfer.

4. Effect of Morphology on Pressure Drop

One of the thermodynamic properties of porous media is pressure drop. Accurate prediction of pressure drop is very important for designing heat exchangers and reactors using porous structures. In this section, a number of correlations given in the literature for predicting pressure drop of porous structures, including metal foam, lattice-frame structures, and other porous media, are reviewed.

4.1 Pressure drop correlations for open-cell foam structures

Fluid flow regimes are divided into pre-Darcy, Darcy, Forchheimer. and turbulent [118, 119]; there can also be transitional flow between two adjacent regimes. Few authors have investigated pre-Darcy regimes. Dukhan et al. [119] found that the range of pre-Darcy is $Re < 0.4$ for aluminum with 20 PPI, ε_o=0.87, velocity increases with a reduction in pressure drop. For Darcy regimes, the correlation for predicting pressure drop can be given by Eq. (35):

$$\frac{\Delta P}{\Delta l} = \frac{\mu}{K_D} u \tag{35}$$

where ΔP is pressure drop; Δl is the length along the flow direction of the foam structure; μ is dynamic velocity; u is velocity, and K_D is the Darcy permeability of the foam structure. The correlation can be used at low Reynolds numbers. However, for post-Darcy regimes like Forchheimer and turbulent regimes, Forchheimer equations are always used to describe pressure drop, as in Eq. (36):

$$\frac{\Delta P}{\Delta l} = \frac{\mu}{K_D} u + C\rho u^2 \tag{36}$$

where C is the inertia coefficient. However, some authors [120–122] used $\frac{F}{\sqrt{K_D}}$ to replace C, where F is the Forchheimer coefficient. Other authors used the cubic law to describe transition regimes [53], as in Eq. (37):

$$\frac{\Delta P}{\Delta l} = \frac{\mu}{K_D} u + \frac{\gamma\rho}{\mu} \rho u^2 \tag{37}$$

where γ is a dimensionless parameter. Kumar et al. [123] note that the Reynolds number range of transitional regimes is very small and it is difficult to control velocity during experiments. There is therefore almost no literature using the cubic law for predicting pressure drop.

The interpretation of the Forchheimer equation presented by Ergun and Orning [124] is widely accepted by others. Ergun and Orning developed this equation to predict pressure drop over packed beds. The basic form of the Ergun equation [48, 125] is given in Eq. (38):

$$\frac{\Delta P}{\Delta l} = \alpha \frac{S_v^2 (1-\varepsilon_o)^2}{\varepsilon_o^3} \mu u + \beta \frac{S_v (1-\varepsilon_o)}{\varepsilon_o^3} \rho u^2 \tag{38}$$

where α and β are viscous and inertial coefficients respectively. This equation can also be given as follows:

$$\frac{\Delta P}{\Delta l} = \alpha \frac{(1-\varepsilon_o)^2}{\varepsilon_o^3} \frac{1}{d_p^2} \mu u + \beta \frac{(1-\varepsilon_o)}{\varepsilon_o^3} \frac{1}{d_p} \rho u^2 \tag{39}$$

The Ergun equations have been widely used by many authors for development of pressure drop correlations for foam structures.

Several correlations have been developed by different authors, using different methods, and reviews and comparisons have also been published. For example, Dietrich et al. [126] reviewed previously-published pressure data, drawing comparisons with the correlation developed by the authors, which can predict pressure drop within a range of $10^{-1}<Re<10^{5}$ and an error range of ±40%. The velocity range of previous pressure drop data was found to be 0 m/s to 20 m/s. Edourard et al. [127] reviewed pressure drop correlations for foam structures, finding that no correlation works perfectly and that some may be subject to significant error. Kumar et al. [128] reviewed correlations with three different kinds of coefficient: (1) constant Ergun parameters, (2) no constant Ergun parameter, (3) without Ergun-like model, and using new morphological parameters to determine permeability K and F. Based on these reviews, no simple, accurate, uniform correlation for predicting pressure drop could be identified, and previously-published data is varied. Kumar et al. [123] considered the cause of these data variations to be lack of uniformity in the methods used to obtain pressure drop, the methods used to treat data, the choice and definition of morphological, and flow law characteristics, and the choice of characteristic length. Furthermore, Dukhan et al. [118, 119] found that permeability K and F vary with different flow regimes. The choice of different velocity ranges during experiments will hence lead to different predictive correlations.

As shown in Table 3, correlations based on experimental data were reviewed and determined with the range of K in 1.03 to 1420, and the range of C is within 110.24 to 5460. There are wide variations in K and C, caused by the different morphological parameters of foam structures. Comparing Eq. (36) with Eqs. (38) and (39), the following can be obtained:

$$K=\frac{\varepsilon_o^3}{\alpha S_v^2\left(1-\varepsilon_o\right)^2},\quad K=\frac{\varepsilon_o^3 d_p^2}{E_1\left(1-\varepsilon_o\right)^2},$$

$$C=\beta\frac{S_v\left(1-\varepsilon_o\right)}{\varepsilon_o^3},\quad C=E_1\frac{\left(1-\varepsilon_o\right)}{\varepsilon_o^3}\frac{1}{d_p}$$

We find that K increases with increasing ε_o and characteristic lengths (d_p, d_h, d_s, D_p, d_c etc. have different definitions); K increases with decreasing S_v, while C increases with increasing S_v, and decreasing ε_o and characteristic length. However, the definitions of K and C only provide an approximate value, and can't be used at all open-cell foam. Therefore, it is essential to develop correlations for specific foam used at engineering application.

Furthermore, as shown in Table 3, the range of experimental velocity is within 0 m/s to 20 m/s, and most authors investigated the range of 0 m/s to 10 m/s. Experimental data from various sources are summarized in Fig. 13. Because of the non-uniform definition of Reynolds number Re and Hagen number Hg, this work summarized the original experimental data of pressure drop vs. velocity. Fig. 13 gives the same conclusion as Table 3, with the range of experimental velocity being 0 m/s to 20 m/s. There are therefore few experimental data for turbulence regions. For the design of heat exchangers to be used under high Reynolds number conditions, there is a need for pressure drop experimental data under high velocity conditions. For a deep understand of the difference of various correlations in high Reynolds number, the predictive curves of correlations developed by different authors are shown in Figs. 14 and 15. The velocity ranges are set within 0 m/s to 10 m/s and 0 m/s to 50 m/s, respectively; the morphological parameters of the sample are assumed to be ε_o=0.91, PPI=20, $d_s=2\times10^{-4}$, and $d_w=1\times10^{-3}$ respectively. Other morphological parameters in correlations are calculated using definitions given by different authors. From Figs. 14 and 15, the deviation among all correlations are huge even blow 10 m/s. Furthermore, the pressure drop prediction difference between Liu [74] and Topin [129] is 302 816.73 Pa/m at 10 m/s; the gap increases with an increase in velocity, to 3 572 914.22 Pa/m at 50 m/s. These correlations have different ranges of application, but the increase in difference with increase in velocity shows that it is hard to predict pressure drop under high Reynolds number conditions in the region of turbulence. Therefore, the more attention should be paid on the investigation of higher Reynolds number to face specially application such as aerospace.

From the above analysis, the following conclusions can be drawn:

(1) The flow law for different flow regions should be chosen before developing the pressure drop prediction correlation.

(2) Forchheimer and Ergun equations are mostly used in post-Darcy regions, to develop pressure drop prediction correlations for open-cell foam structures.

(3) There is no generally-applicable correlation to predict pressure drop for a given sample.

(4) There is a strong need for correlations to be developed for turbulence regions with high Reynolds numbers.

4.2 Pressure drop correlations of lattice-frame structures

Although there are many pressure drop correlations for open-cell foam structures, only few authors give correlations for lattice-frame structures. In this case, due to the regular periodic structure, it is easy to obtain more accurate correlations.

Table 3 Pressure drop correlation

Author	Simple	ε_o	PPI	D_p/mm	d_s/mm	$K\times10^{-9}$/m^2	C/m^{-1}	Correlation	Range of investigate velocity/m·s^{-1}
Du Plessis et al. [69]	G100	0.973	100	0.1265	0.047	1.77	2247	$\frac{\Delta P}{\Delta l}=\frac{36\chi(\chi-1)}{\varepsilon_0^2 D_p^2}\mu u+\frac{2.05\chi(\chi-1)}{\varepsilon_0^2(3-\chi)D_p}\rho u^2$ $\frac{1}{\chi}=\frac{3}{4\varepsilon_o}+\frac{\sqrt{9-8\varepsilon_o}}{2\varepsilon_o}\times\cos\left\{\frac{4\pi}{3}+\frac{1}{3}\cos^{-1}\left[\frac{8\varepsilon_o^2-36\varepsilon_o+27}{(9-8\varepsilon_o)^{3/2}}\right]\right\}$	0–0.7 (glycerol) 0–0.16 (water)
	G60	0.975	60	0.2609	0.054	8.00	1023		
	G45	0.978	45	0.3568	0.054	16.02	695		
Richardson et al. [59]	Al_2O_3	0.878	10	1.68	–	19.251	110.24	$\frac{\Delta P}{\Delta l}=E_1\frac{S_v^2(1-\varepsilon_o)^2}{\varepsilon_o^3}\mu u+E_2\frac{S_v(1-\varepsilon_o)}{\varepsilon_o^3}\rho u^2$ $E_1=973D_p^{0.743}(1-\varepsilon_o)^{-0.0982}\quad E_2=368D_p^{-0.7523}(1-\varepsilon_o)^{-0.07158}$	0.7–6 (air)
		0.874	30	0.826		4.821	560.72		
		0.802	45	0.619		3.963	921.62		
		0.857	65	0.359		2.395	1765.72		
Moreira et al. [25]	SiC-Al_2O_3	0.94	8	2.30	–	363.00	302.59	$\frac{\Delta P}{\Delta l}=1.36\times10^8\frac{(1-\varepsilon_o)^2}{\varepsilon_o^3 D_p^{0.264}}\mu u+1.8\times10^4\frac{(1-\varepsilon_o)}{\varepsilon_o^3 D_p^{-0.24}}\rho u^2$	0–20 (air) 0–0.35 (water)
		0.88	20	0.80		60.18	572.46		
		0.76	45	0.36		9.09	1467.42		
Giani et al. [27]	Fe-alloy	0.927	5.4	4.70	0.82	40.11	202.56	$\frac{\Delta P}{\Delta l}=\frac{26.12}{d_s^2}\left(\frac{1}{1-G}\right)^4\frac{G}{4}\mu u+\frac{1.74}{d_s}\left(\frac{1}{1-G}\right)^4\frac{G}{4}\rho u^2$ $G=2\left[(1-\varepsilon_o)/3\pi\right]^{1/2}$	1–16 (air)
		0.938	11.5	2.20	0.37	46.51	387.12		
		0.937	12.8	2.00	0.33	45.85	440.26		
		0.911	5.6	4.60	0.80	33.20	250.85		
Dietrich et al. [23, 126]	Al_2O_3	0.690	20	0.218	0.0651	130	1136.36	$\frac{\Delta P}{\Delta l}=\frac{110}{\varepsilon_o d_h^2}\mu u+\frac{1.45}{\varepsilon_o^2 d_h}\rho u^2$	1–10 (air)
		0.765	10	0.322	0.0967	77	534.76		
		0.748	20	0.1567	0.0476	54	877.19		
		0.752	30	0.1275	0.0391	32	1020.41		
		0.757	45	0.082	0.0195	20	1315.79		
		0.811	20	0.2008	0.0544	144	555.56		
	Mullite	0.741	20	0.1992	0.0612	90	1050.63		
			10	0.3006	0.0895	299	537.63		
			20	0.195	0.0545	88	819.67		
		0.748	30	0.166	0.0533	45	980.39		
		0.744	45	0.0973	0.0293	29	1515.15		
			20	0.2032	0.051	120	529.32		
	OBSiC		20	0.2257	0.0896	65	1052.63		
			10	0.332	0.1063	276	740.74		
			20	0.2208	0.0719	56	813.01		
			30	0.1651	0.0544	46	1190.48		
			45	0.099	0.0275	17	2000.00		
			20	0.7687	0.0622	220	666.67		

Continued Table 3

Author	Simple	ε_o	*PPI*	D_p/mm	d_s/mm	$K\times10^{-9}$/m^2	C/m^{-1}	Correlation	Range of investigate velocity/m·s^{-1}
Dukhan et al. [130, 131]	Al	0.919	10	–	0.406	100	210	10 PPI $K=10^{-8}\left(0.0013e^{9.55\varepsilon_o}\right)$, $C=100\left(-61.33\varepsilon_o+58.362\right)$	0.5–3 (air)
		0.915	10		0.406	80	270		
		0.919	20		0.203	63	290	20 PPI $K=10^{-8}\left(0.0009e^{9.46\varepsilon_o}\right)$, $C=100\left(-114.61\varepsilon_o+108.44\right)$	
		0.924	20		0.203	54	280		
		0.923	40		0.102	47	380	40 PPI $K=10^{-8}\left(8\times10^{-7}e^{16.39\varepsilon_o}\right)$, $C=100\left(-239.92\varepsilon_o+22.51\right)$	
Tadrist et al. [132]	Al	0.917	10	–	1.00	130	128	$\frac{\Delta P}{\Delta l}=\alpha\frac{\left(1-\varepsilon_o\right)^2}{\varepsilon_o^3 d_s^2}\mu u+\beta\frac{\left(1-\varepsilon_o\right)}{\varepsilon_o^3 d_s}\rho u^2$	–
		0.933	20		0.86	250	240		
		0.905	40		0.69	66	389	$100<\alpha<865;\quad 0.65<\beta<2.6$	
Mancin et al. [20]	Al	0.921	5	5.08	0.540	236	205	$\frac{\Delta P}{\Delta l}=\frac{2FG^2}{\rho d_h}\quad G=\rho u\quad F=\frac{1.765\,Re^{-0..1014}\,\varepsilon^2}{\mathrm{PPI}^{0.6}}$	2–6 (air)
		0.903	10	2.54	0.529	190	170		
		0.934	10	2.54	0.450	187	190		
		0.956	10	2.54	0.445	182	240	$Re=\frac{d_h G}{\mu\varepsilon}\quad d_h=0.0122\times\mathrm{PPI}^{-0.849}$	
		0.932	20	1..27	0.367	82.4	226		
		0.930	40	0.635	0.324	63.4	342		
Lacroix et al. [29]	SiC	0.915	–	–	0.143	32.5	905	$\frac{\Delta P}{\Delta l}=150\frac{\left(1-\varepsilon_o\right)^2}{\varepsilon_o^3 d_p^2}\mu u+1.75\frac{\left(1-\varepsilon_o\right)}{\varepsilon_o^3 d_p}\rho u^2$	0–5 (air)
		0.910			0.143	28.5	974		
		0.914			0.390	236	337		
		0.890			0.103	9.27	177	$d_p=1.5d_s$	
		0.810			0.110	2.67	379		
Khayargoli et al. [133]	NC	0.86	–	0.4	–	1.79	2256	$\frac{\Delta P}{\Delta l}=100\frac{\left(1-\varepsilon_o\right)^2}{\varepsilon_o^3 d_p^2}\mu u+\frac{\left(1-\varepsilon_o\right)}{\varepsilon_o^3 d_p}\rho u^2$	0–15 (air)
		0.83		0.5		3.39	1755		
		0.9		0.6		4.76	374		
	NCX	0.89		0.9		15.41	483	$d_p=1.5\frac{\left(1-\varepsilon_o\right)}{\varepsilon_o}D_p$	
		0.9		1.4		27.64	374		
Wu et al. [134]	AS	0.55	–	–	–	3.12	5460	$\frac{\Delta P}{\Delta l}=\frac{\left(1039-1002\varepsilon_o\right)}{d_c^2}\mu u+\frac{0.5138\varepsilon_o^{-5.739}}{d_c}\rho u^2$	0–10 (air)
		0.7				5.52	2360		
		0.85				1.03	893		
		0.7				2.17	990		
		0.7				3.03	662		
Topin et al. [129]	NC	–	–	–	–	Water / air	Water / air	$\frac{\Delta P}{\Delta l}=1.391\times10^{-4}\frac{\left(1-\varepsilon_o\right)^2}{\varepsilon_o^3 D_p^2}\mu u+1.32S_v\rho u^2$	(water) 0–2 (air)
		0.90	–	40	–	2.28 / 1.85	2194 / 2138		
		0.87	–	569	–	2.68 / 2.13	1622 / 1330		
		0.91	–	831	–	6.19 / 4.44	1130 / 1075		
		0.88	–	1840	–	23.2 / 28.1	631 / 490		
		0.89	–	2452	–	29.8 / 60.2	400 / 381		

Continued Table 3

Author	Simple	ε_o	*PPI*	D_p/mm	d_s/mm	$K\times10^{-9}$/m^2	C/m^{-1}	Correlation	Range of investigate velocity/m·s^{-1}
Liu et al. [74]	Al	0.914	5	1.21	–	370	164.07	$\frac{\Delta P}{\Delta l}=\frac{22(1-\varepsilon_o)^2}{\varepsilon_o^3 d_p^2}\mu u+\frac{0.22(1-\varepsilon_o)}{\varepsilon_o^3 d_p}\rho u^2$	0–10 (air)
		0.918	10	1.19		623	230.58		
		0.870	20	8.27		125	280.86		
		0.909	20	8.05		102	231.08		
		0.935	20	8.14		242	264.26		
		0.958	20	8.00		1420	285.32		
		0.935	40	6.85		133	282.43		
Inayat et al. [135]	Ti-6Al-4V	0.871	–	4.189	1.104	–	–	$\frac{\Delta P}{\Delta l}=\frac{\alpha}{36}\frac{S_v^2}{\varepsilon_o^3}\mu u+\frac{\beta}{6}\frac{S_v}{\varepsilon_o^3}\rho u^2$ $\alpha=\left[\left(\frac{1-0.971(1-\varepsilon_o)^{0.5}}{0.6164(1-\varepsilon_o)^{0.5}}\right)\varepsilon_o\right]^{-1}$ $\beta=\left[\left(\frac{1-0.971(1-\varepsilon_o)^{0.5}}{0.6164(1-\varepsilon_o)^{0.5}}\right)(1-\varepsilon_o)\right]^{-1}$	0–6 (air)
		0.846	–	3.413	1.016				
		0.799		2.688	0.999				

4.2.1 Tetrahedral structure

Kim et al. [9, 137, 138] investigated the hydraulic characteristics of tetrahedral structures, defining unit cell length S_{cell} (as shown in Fig. 7, this is S_x for the x direction, and S_y for the y direction) as characteristic length. They used a pressure loss coefficient per unit cell K_{cell} based on periodic flow patterns, as in Eq. (40):

$$K_{cell}=\frac{\Delta P_{cell}}{\rho u^2/2} \tag{40}$$

where ΔP_{cell} is pressure drop per unit cell. Through experiments, the authors obtained the following correlations:

$$K_{cell}=1000\frac{1}{Re_{S_{cell}}},\quad Re_{S_{cell}}<2000 \tag{41}$$

Transition range: $2000<Re_{S_{cell}}<3000$, K_{cell}=0.32 for x direction, K_{cell}=0.62 for y direction: $3000<Re_{S_{cell}}$. The same trends were noted by Son et al. [38].

4.2.2 Pyramidal and Kagome structure

Krishnan et al. [139] numerically investigated Tetrahedral, Pyramidal, and Kagome structures, concluding that the friction factor (f) values vs. Reynolds number of these three structures, were ranked according to select flow direction as: Kagome>Pyramidal>Tetrahedral. Hoffmann [140] also defined a correlation for predicting pressure drop in Kagome structures in the region of turbulence, given in Eq. (42):

$$f=\frac{\Delta P}{L}\frac{H}{\rho u^2/2}=0.56 \tag{42}$$

4.2.3 X-type structure

For X-type structures, Yan et al. [83] found that the f value of 2.58 is constant within 1400<Re_H<7500.

Although the periodic nature of the lattice-frame structure allows for development of accurate pressure drop correlations, more extensive dynamic experiments for these structures with different morphological parameters are needed.

4.3 Pressure drop in structured packed beds and wire-woven structures

4.3.1 Packed beds

For the prediction of pressure drop in packed beds, Ergun [124] developed the most widely used correlation, given by Eq. (39), where E_1 and E_2 are 150 and 1.75 respectively; Eq. (39) can be transformed to Eq. (43), as shown:

$$f=150\frac{(1-\varepsilon)}{Re}+1.75 \tag{43}$$

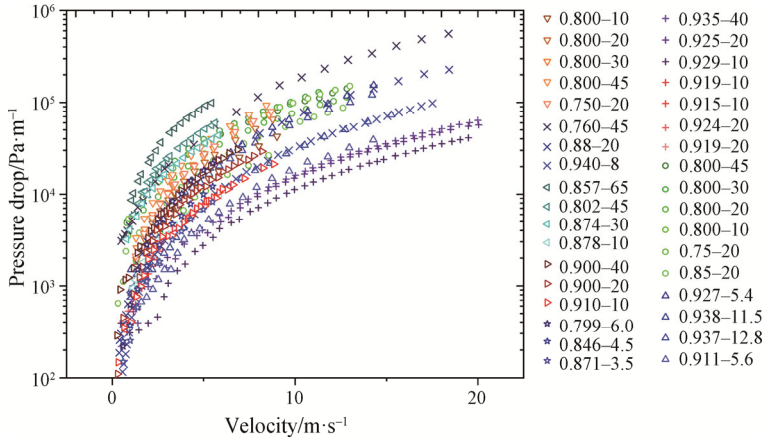

Fig. 13 Pressure drop vs velocity of various foam: (1) Dukhan-11 (Al) [39], (2) Dukhan-06 (Al) [130], (3) Garrido-08 (Al_2O_3) [37], (4) Giani-05 (Fe-alloy) [27], (5) Dietrich-09 (Al_2O_3) [23], (6) Moreira-04 (SiC-Al_2O_3) [26], (7) Richardson-00 (Al_2O_3) [59], (8) Leong-06 (Al) [136], (9) Inayat-11 (Ti-6Al-4V) [135]. The experimental velocity is within 0 m/s to 20 m/s, and most authors investigate the range of 0 m/s to 10 m/s

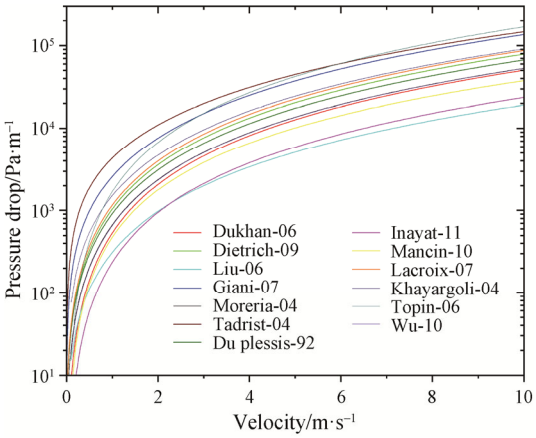

Fig. 14 Pressure drop vs velocity prediction with different correlation developed by different author within 0–10 m/s. The morphological parameters of the sample are assumed to be ε_o=0.91, PPI=20, d_s=2×10^{-4}, and d_w = 1×10^{-3}, respectively

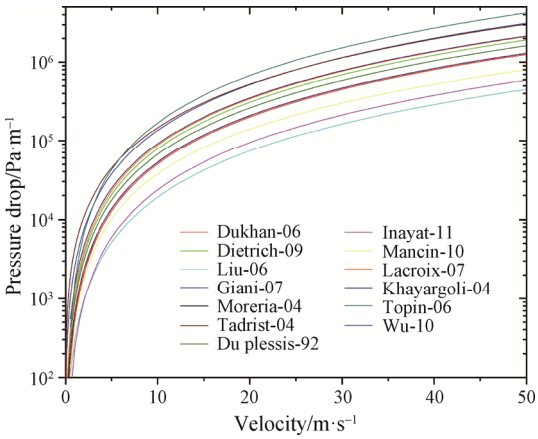

Fig. 15 Pressure drop vs velocity prediction with different correlation developed by different author within 0–50 m/s. The morphological parameters of the sample are assumed to be ε_o=0.91, PPI=20, d_s=2×10^{-4}, and d_w = 1×10^{-3} respectively

where $f = \dfrac{\Delta P}{L}\dfrac{d_p}{\rho u^2}\dfrac{\varepsilon^3}{(1-\varepsilon)}$ and Reynolds number $Re = \dfrac{d_p \rho u}{\mu}$. Many correlations have almost the same formation as Eq. (43). This can also be modified as follows:

$$f = c_1 \frac{(1-\varepsilon)}{Re} + c_2 \tag{44}$$

where c_1 and c_2 are constant; in some correlations c_1 and c_2 are related to ε. Erdim et al. [141] reviewed many pressure drop correlations for packed beds and related Re ranges of application. They concluded that, although many new correlations have been developed, few authors have compared and evaluated existing correlations widely enough. There is therefore no general agreement on which correlations are the most accurate. However, the random packed beds always show a huge pressure drop due to the lower porosity and complex air pathways. Therefore, the packed methods have been investigated to decrease pressure drop.

For structured packed beds, the Ergun correlation over predicted pressure drop [142]. The flow pressure drop in structured beds is much lower than that in random packed beds. Furthermore, pressure drop is closely connected with packing form [97, 143]. Susskind et al. [144] investigated flow in various packing forms, finding that pressure drop decreases with an increase in relative horizontal spacing. Yang et al. [145] numerically

investigated five different packed channels, finding that pressure drop will greatly decrease and overall heat transfer performance will increase, given well-selected packing form. Wang et al. [98] developed a new packing form (the GSCSPB) and investigated its pressure drop and overall heat transfer performance. For heat transfer enhancement, structured packed beds have more potential than random structures. Different packing forms can be developed to flexibly satisfy different heat transfer enhancement applications. There should therefore be further investigation of packing forms.

4.3.2 Wire-woven structure

Wire-woven metals have various applications for heat transfer due to their flexible structure. However, only a few structures have been investigated in relation to pressure drop. Tian et al. [146] experimentally investigated the pressure drop of plane weave copper meshes, giving f for different samples in Reynolds number ranges of 700 to 10 000. The authors also found that f is not only a function of ε, but also a function of the open area ratio. Compared with other wire-woven metal structures, wire-woven bulk Kagome (WBK) has been more widely investigated for its pressure drop qualities. The pressure drop properties of single-layered WBK have been numerically investigated by Shen et al. [147], who found its f to be 0.54 in the Reynolds range of 3995 to 8710. The authors also compared the pressure drop with that of Kagome lattice-frame structures, finding that both structures have almost identical pressure drop. For the multi-layered WBK, Joo et al. [148] obtained the f vs. Reynolds number functions for two directions of multi-layered WBK (five layers), given by Eqs. (45) and (46):

A-direction

$$f= -2.608\ln(Re_{\mathrm{H}})+3.0116 \quad 5.5\times10^{3}\le Re_{\mathrm{H}}\le 1.8\times10^{4} \tag{45a}$$

$$f= 0.0645\ln(Re_{\mathrm{H}})-0.1847 \quad 1.8\times10^{4}\le Re_{\mathrm{H}}\le 3.3\times10^{4} \tag{45b}$$

B-direction

$$f= -0.8049\ln(Re_{\mathrm{H}})+8.2254 \quad 5.2\times10^{3}\le Re_{\mathrm{H}}\le 1.7\times10^{4} \tag{46a}$$

$$f= -0.2165\ln(Re_{\mathrm{H}})+2.5497 \quad 1.7\times10^{4}\le Re_{\mathrm{H}}\le 2.5\times10^{4} \tag{46b}$$

$$f= 0.0585\ln(Re_{\mathrm{H}})-0.2570 \quad 2.5\times10^{4}\le Re_{\mathrm{H}}\le 3.1\times10^{4} \tag{46c}$$

where $Re_{D_{\mathrm{h}}}=\dfrac{\rho u D_{\mathrm{h}}}{\mu}$. D_{h} is the hydraulic diameter of a rectangular test section. They also investigated three-layered WBK, obtaining other correlation forms for pressure drop prediction [8], given by Eq. (47):

A-direction

$$f=3120\left(Re_{D_{\mathrm{h}}}\right)^{-1} \quad Re_{D_{\mathrm{h}}}<6000 \tag{47a}$$

B-direction

$$f=3430\left(Re_{D_{\mathrm{h}}}\right)^{-1} \quad 6000<Re_{D_{\mathrm{h}}}<10\,000 \tag{47b}$$

$$\text{Transition region} \quad 6000<Re_{D_{\mathrm{h}}}<10\,000 \tag{47c}$$

The difference in pressure drop between A-direction and B-direction is due to the open area ratio. The A-direction open area ratio (0.75) is larger than that of the B-direction (0.62) [8]. The open area ratio should thus be factored into pressure drop prediction. Furthermore, the pressure drop of wire-woven structure should be compared with lattice-frame structure with the same shape, and figured out the difference between two structures. In addition, many other structures have still not been investigated for their pressure drop properties.

5. Effect of Morphology on HTC

The HTC is an indispensable parameter for heat exchangers, solar energy collection and storage, and cooling systems, and other applications. However, it is hard to predict HTC though theoretical derivation, especially in the case of porous structures. Some authors have therefore combined experimental and numerical analysis to develop HTC correlations. In this section, a number of HTC correlations for open-cell foam, lattice-frame, and other porous structures will be reviewed.

5.1 Correlations for predicting HTC of open-cell foam structures

It is important to understand transport properties at pore scale in open-cell foam structures. These can explain macroscopic heat transfer phenomena and can also offer methods of optimizing pore scale structure design for different applications. However, it is hard to determine microscopic properties through experimentation due to the complexities of pore scale structure. The volume averaging method is generally used to analyze heat transfer in open-cell foam structures. This method is applied if the pore size of porous media is much smaller than the scale of the research system [149]. Two types of models are used to apply the volume average method in investigating heat transfer: local thermal equilibrium (LTE) and local thermal non-equilibrium (LTNE) models [150]. LTE models are also referred as one-equation models; these are always used under conditions of small local temperature

differences between fluid and solid. However, in many applications, local temperature differences are larger and in these situations, the LTNE model (two-energy equation) is applied. The LTNE energy equations can be divided into fluid energy and solid energy equations, given in Eqs. (48) and (49), respectively:

Fluid energy:

$$\varepsilon\left(\rho c_p\right)_{\mathrm{f}}\frac{\partial T_{\mathrm{f}}}{\partial t}+\left(\rho c_{\mathrm{p}}\right)_{\mathrm{f}} v\cdot\nabla T_{\mathrm{f}} = \nabla\cdot\left(\underline{K}\cdot\nabla T_{\mathrm{f}}\right)-h_{\mathrm{v}}\left(T_{\mathrm{f}}-T_{\mathrm{s}}\right) \tag{48}$$

Solid energy:

$$\left(1-\varepsilon\right)\left(\rho c\right)_{\mathrm{s}}\frac{\partial T_{\mathrm{s}}}{\partial t}=\nabla\cdot\left(\underline{K}\cdot\nabla T_{\mathrm{f}}\right)-h_{\mathrm{v}}\left(T_{\mathrm{s}}-T_{\mathrm{f}}\right) \tag{49}$$

where $\underline{K}$ is total effective thermal conductivity tensor, and h_{v} is volumetric heat transfer coefficient (VHTC). VHTC couples the fluid energy and solid energy equations.

There are three ways to obtain VHTC: experimentally, through theoretical derivation [151], or through numerical simulation [65, 152]. Experimental methods can be divided into steady state [7] and transient methods (single-blow method) [28, 120, 153]. VHTC values obtained using steady state methods are affected by the thermal conductivity of open-cell foam; while in the case of transient methods, the temperature difference can be neglected in the transverse direction [7, 28]. Xia et al. [28] also noted that transient methods are simpler in their operation than steady state methods. A few authors have obtained VHTC through theoretical derivation, due to the complexities of pore scale structure. Nakayama et al. [151] developed a correlation for predicting VHTC (given in Table 4) through rigorous mathematical derivation. Many authors have used numerical simulation to develop correlations for predicting VHTC. One group of authors used the real structure of open-cell foam obtained through computer tomography, and used CFD to simulate the heat transfer characteristics of open-cell foam. However, the scale of reconstructed structures is always small and these cannot model fluid lateral mixing in open-cell foam very well. Another group of authors used simplified geometry, such as cubic [154] dodecahedron [155] tetrakaidecahedral models [152, 156]. Although these can give a large scale through the use of a periodic boundary, such models still differ from the real structures. The transient methods are most of the methods used by authors due to the reliable theoretical basis, simple experimental process and less influence factors.

This present work reviewed several VHTC-predicting correlations developed in different ways. As shown in columns 2, 3, and 4 of Table 4, many samples with a large range of ε (0.65 to 0.97) and PPI (5 to 66.04) have been investigated. As in the case of pressure drop predicting correlations, from column 5 of Table 4 it can be noted that there is no unique characteristic length for VHTC correlations. d_{w} and d_{s} are widely used as characteristic length, due to the ease of determination. Furthermore, Fu et al. [157] developed four VHTC predictive correlations with four different characteristic lengths: d_{h}, d_{m}, $1/S_{\mathrm{v}}$, and d_{r}. The characteristic length $1/S_{\mathrm{v}}$ is also used by Peng et al. [158]. Dietrich [22] used hydraulic diameter d_{h} as characteristic length, but this is defined differently than by Fu et al. Although, the VHTC predictive correlation used d_{h}, d_{m} also showed a good agreement with experimental data in their own work, as discussion in section 3, the errors of d_{s}, ε_{o}, S_{v} and PPI will influence accuracy of pore diameter. And then, the correlations are hard to use to predict VHTC for other open-cell foam accurately. From column 7, it can be noted that the investigative range of velocity is below 10 m/s; the VHTC of turbulence regions with velocities higher than 10 m/s therefore remains to be investigated. Some predictive correlations of interstitial Nusselt number $Nu=\dfrac{hl}{k_{\mathrm{f}}}$ and volumetric Nusselt number $Nu=\dfrac{h_{\mathrm{v}}l^2}{k_{\mathrm{f}}}$ are given in column 6, where l is characteristic length, h is interstitial heat transfer coefficient; h_{v} is VHTC, and k_{f} is fluid thermal conductivity. Additionally, if $Nu_{\mathrm{v}}=\dfrac{h_{\mathrm{v}}}{k_{\mathrm{g}}S_{\mathrm{v}}}$ when $1/S_{\mathrm{v}}$ is the characteristic length, the correlation between VHTC h_{v} and interstitial heat transfer coefficient h is $h_{\mathrm{v}}=hS_{\mathrm{v}}$. The form of most correlations can be given as in Eq. (50):

$$Nu_{\mathrm{v}}=a\,Re^{b} \tag{50}$$

where a and b are coefficients. Coefficient a is related to parameters like ε_{o} [151, 152], thickness of porous media H [153, 157], Reynolds number Re [22], and Prandtl number Pr [159, 160], while coefficient b is almost constant. Younis and Viskanta take d_{w}/H into consideration. Hwang et al. [120] developed three different Nusselt number correlations with three different porosities. Ando et al. [161] also developed five correlations for five samples with different PPI*s*. Some authors used different correlation forms; for example, Peng et al. [158] took temperature T and ε_{o} into consideration and used the form: $Nu_{\mathrm{v}}=A+aRe^{b}$, while Dietrich et al. [22] developed Nusselt-Hagen correlations that can allow easy and accurate prediction of HTC based on pressure data of the foam structure. Therefore, different effect were taken into consideration by different authors, and this is the reason why lacking uniform predictive correlations.

Table 4 HTC correlations

Author	samples	ε_o	PPI	Characteristic length	Correlation	Range of Velocity /m·s^{-1}	Method
Younis-Viskanta et al. [153]	Al_2O_3	0.870	10.16	ε_o	$Nu_v = 0.819\left[1-7.33\frac{d_w}{H}\right]Re_{d_w}^{0.36\left[1+15.5\frac{d_w}{H}\right]}$	1.24–6.75	Transient
		0.850	20.34			1.00–7.15	
		0.830	30.48			1.20–6.37	
		0.840	45.72			1.16–6.48	
		0.834	66.04			1.56–5.72	
Fu et al. [157]	YZA	–	10.16	$d_h = 4\varepsilon_o/S_v$ $d_m = \frac{\sqrt{4\varepsilon_o/\pi}}{\mathrm{PPC}}$ $d_s = 1/S_v$ $d_s = C/F$	$Nu_v = \left[0.0730+1.302\left(H/d_h\right)\right]Re_{d_h}$ $Nu_v = \left[0.0426+1.236\left(H/d_m\right)\right]Re_{d_m}$ $Nu_v = \left[0.0252+1.280\left(H/d_a\right)\right]Re_{d_a}$ $Nu_v = \left[0.000267+1.447\left(H/d_r\right)\right]Re_{d_r}$	0.08–6.00	Transient
			20.34				
			30.48				
	SiC		20.34				
	Mullite		20.34				
			20.34				
	Cordierite		45.72				
			66.04				
Hwang et al. [120]	Al	0.700	–	d_w	$Nu_v = 0.1569\,Re_{d_w}^{0.825}$	0.40–2.00	Transient
		0.800			$Nu_v = 0.3560\,Re_{d_w}^{0.644}$		
		0.950			$Nu_v = 0.3248\,Re_{d_w}^{0.601}$		
Giani et al. [27]	Fe-Cr alloy	0.927	5.4	d_s	$Nu_v = 1.2\,Re_{d_s}^{0.43}\,Pr^{1/3}$	1.20–5.70	Transient
		0.937	12.8				
	Cu	0.911	5.6				
Calmidi et al. [160]	Al	0.9726	5	d_s	$Nu_v = 0.52\,Re_{d_s}^{0.5}\,Pr^{0.37}$	0.61–3.20	steady
		0.9118	5				
		0.9486	10				
		0.9546	20				
		0.9005	20				
		0.9272	40				
		0.9132	40				
Nakayama et al. [151]	–	0.70–0.95	–	d_c	$Nu_v = 0.07\left(\frac{\varepsilon}{1-\varepsilon}\right)^{2/3}Re_{d_c}\,Pr^{0.37}$	–	Theoretical derivation
Wu et al. [152]	–	0.66–0.93	–	d_c	$Nu_v = 2.069S_v\varepsilon_o^{0.38}\,Re_{d_c}^{0.438}$	0.60–8.00	Numerical simulations
Ando et al. [161]	Ceramic	–	6	d_w	$Nu_v = 0.055\,Re_{d_w}^{1.15}$ $Nu_v = 0.012\,Re_{d_w}^{1.27}$ $Nu_v = 0.015\,Re_{d_w}^{1.21}$ $Nu_v = 0.342\,Re_{d_w}^{0.80}$	1.00–10.00	Transient
			9				
			13				
			20				

Continued Table 4

Author	samples	ε_o	*PPI*	Characteristic length	Correlation	Range of Velocity (m/s)	Method
Dietrich [22]	Al_2O_3	0.800	10	$d_h = 4\frac{\varepsilon_o}{S_v}$	$Nu = 0.45 C_{Re} C_{geo} Hg_{d_h} Pr^{1/3}$ $Nu = 0.57 C_{Re} C_{geo} Re_{d_h} Pr^{1/3}$ $Hg_{d_h} = \frac{\Delta P}{\Delta L}\frac{d_h^3}{\rho_f u^2}$ $C_{Re} = \left(\frac{Re+1}{Re+100}\right)^{0.25}$ $C_{geo} = \left(\frac{d_h/L}{(d_h/L)_{mean}}\right)^{1.5}$	0.50–5.00	Transient
		0.800	20				
		0.800	30				
		0.800	45				
		0.750	20				
		0.850	20				
	OBSiC	0.800	10				
		0.800	20				
		0.800	30				
		0.800	45				
		0.750	20				
		0.850	20				
	Mullite	0.800	10				
		0.800	20				
		0.800	30				
		0.800	45				
		0.750	20				
		0.850	20				
Peng et al. [158]	Al_2O_3	0.995	30	$1/S_v$	$Nu_v = 3.43\times10^{-11}\varepsilon_o T^3 + 0.0340\, Re_{S_v}$	0.60–1.00	Steady
Kamiuto et al. [163]	RD	RD	RD	d_s	$Nu_v = 0.124\left(Re_{d_s} Pr\right)^{0.791}$	0.05–15	Transient and steady
Xia et al. [28]	Cu	0.900	10	d_w	$Nu_v = 0.34\varepsilon_o^{-2} Re_{d_w}^{0.61} Pr^{1/3}$	2.00–9.00	Transient
		0.900	20				
	Ni	0.900	10				
		0.900	20				
		0.900	40				
		0.970	20				
		0.870	20				
	SiC	0.88	10				
		0.88	20				

RD: Review data

This present work reviewed experimental data of VHTC vs. velocity; as shown in Fig. 16, the obtained data were mostly within a velocity range of 0 m/s to 10 m/s. It is also noted that some data obtained differ from those given by other authors by some orders of magnitude, even at the same velocity. As in the case of experimental pressure data, discussed in the previous section, there are few experimental VHTC data for turbulence regions. Future work should thus focus on obtaining the VHTC of open-cell foam structures at high Reynolds number ranges. Fig. 17 summarizes the predictive curve of some VHTC correlations. Some assumed conditions are given: the morphological parameters of the sample are set as ε_o=0.95, PPI=20, d_s=2×10^{-4}, d_w=1×10^{-3} respectively; other morphological parameters in correlations are calculated using different definitions given by different authors. The velocity ranges are set to 0 m/s to 10 m/s and 0 m/s to 50 m/s, respectively. From Figs. 17 and 18, an increase in difference with velocity can be noted; for example, the VHTC values predicted by Xia [28] and Fu [157] are 32 728.61 kW/(m^3·K) and 164 077.8 kW/(m^3·K) at 10 m/s and 50 m/s, respectively. Furthermore, some curves cross in the predicting velocity range. Differences between correlations may result from using different methods to develop correlations, from different shapes and materials of samples, or from different experimental conditions. There is thus no general correlation for predicting the VHTC of open-cell foam structures in the turbulence region with high Reynolds numbers. It is noteworthy that the above correlations are not distinguished according to flow region (Darcy and non-Darcy). Dukhan et al. [162] found that the Nusselt number is constant in the Darcy region.

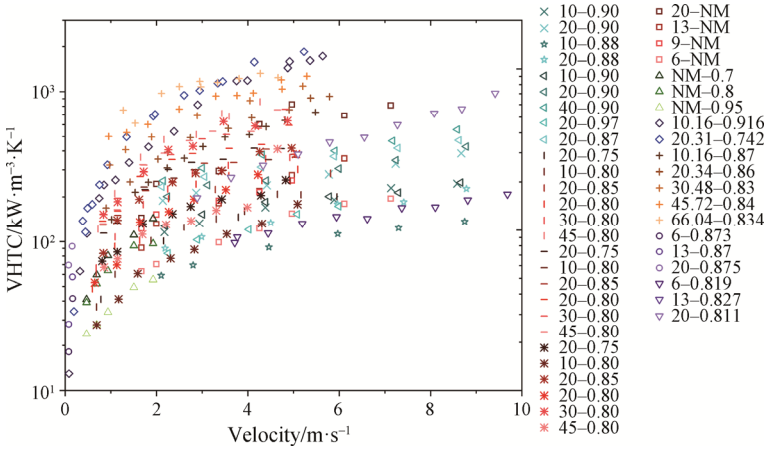

Fig. 16 Data of VHTC vs. velocity: (1) Xia-17 (Cu, SiC, Ni) [28]; (2) Diretch-13 (Al_2O_3, OBSiC, Mullite) [22]; (3) Ando-13 (Al_2O_3) [161]; (4) Hwang-02 (Al) [120]; (5) Fu-98 (YZA) [157]; (6) Younis-Viskanta-93 (Al_2O_3) [153]; (7) Ichimiya-99 (Al-Ceramic) [164]; (8) Kamiuto-05 (Al-Ceramic) [163]

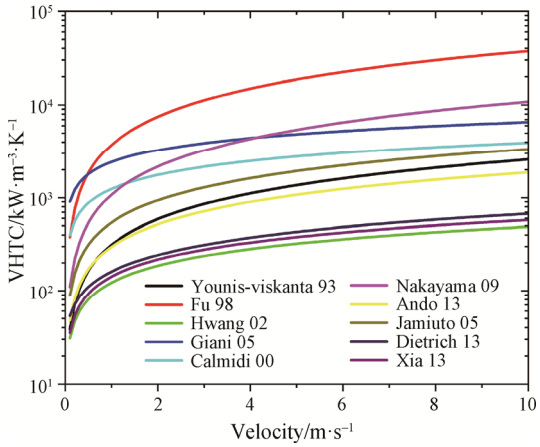

Fig. 17 VHTC vs. velocity prediction with different correlation developed by different author within 0 m/s to 10 m/s

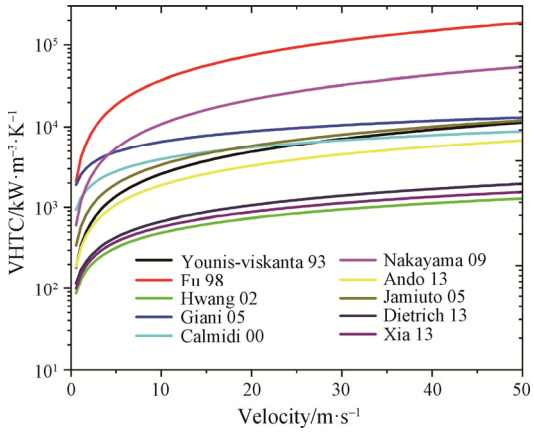

Fig. 18 VHTC vs. velocity prediction with different correlation developed by different author within 0 m/s to 50 m/s

From the above analysis, it can be concluded that:

(1) LTNE models are used for application of the volume average method in investigating heat transfer of open-cell foam structures.

(2) Transient experiments are most widely used by authors to determine VHTC.

(3) There are no generally-applicable VHTC predictive correlations.

(4) There is a need for development of correlations that can be applied in turbulence regions with high Reynolds numbers.

5.2 Correlations for predicting HTC of lattice-frame structures

5.2.1 Tetrahedral structure

As in the case of pressure drop correlations, there are few HTC correlations for lattice-frame structures. Kim et al. [137, 138] investigated forced convection heat transfer of single-side heating tetrahedral structures. Correlations for predicting the spatially-averaged HTC for different materials in the y direction (shown in Fig. 7) were developed [138], given in Eq. (51):

LM25 core and substrates

$$Nu_{S_y} = 1.02\, Re_{S_y}^{0.55} \tag{51a}$$

Polycarbonate core with Al substrates

$$Nu_{S_y} = 0.14\, Re_{S_y}^{0.68} \tag{51b}$$

The authors found that the tetrahedral structure contributed 57% of overall heat transfer when using a high thermal conductivity material. In the x direction, the spatially-averaged HTC predictive correlation for LM25 core and substrates [9] is as shown in Eq. (52):

$$Nu_{S_y} = 0.98\, Re_{S_y}^{0.56} \tag{52}$$

The authors also analyzed the influence of flow characteristic of the tetrahedral structure on overall heat transfer [137], with arch-shaped vortices, horseshoe vortices, and the delay of flow separation was found to contribute to an increase in overall heat transfer. Other authors also investigated tetrahedral structures. Zhang et al. [165] numerically investigated such structures with different strut shapes, i.e., cylinder-shaped and rectangular-shaped struts. For a given Reynolds number, the tetrahedral structure with rectangular-shaped struts has higher overall Nusselt numbers than that with cylinder-shaped struts. Son et al. [38] experimentally investigated forced convection heat transfer of tetrahedral structures with heating on both sides. They correlated strut diameter with ε, as in Eq. (28), finding that the Nusselt number increases with a decrease in ε for a given Reynolds number.

5.2.2 X-type structure

Jin et al. [166] compared the average overall Nusselt number of X-type structures with that of pyramidal structures for a given Reynolds number. X-type structures contributed 47% to 60% higher Nusselt numbers than pyramidal structures. Krishnan et al. [139] compared the Nusselt number of a tetrahedral, pyramidal, and Kagome structure for a given direction and Reynolds number, finding that the Nusselt number rank is as follows: Tetrahedral>Pyramidal>Kagome. Shen et al. [147] compared the overall Nusselt number of Kagome and single-layered wire-woven bulk Kagome (WBK) structures, concluding that the Kagome structure provided 26% to 31% higher overall Nusselt numbers than WBK in the Reynolds number range of 3995 to 8710. Hoffmann et al. [140] developed a correlation for predicting average HTC, given in Eq. (53):

$$Nu_{\mathrm{H}} = 1.3513\, Re_{S_y}^{0.5414} \tag{53}$$

Yan et al. [31, 167] developed a correlation for predicting HTC in X-type structures, given in Eq. (54):

$$Nu_{\mathrm{H}} = 3.228\, Re_{S_y}^{0.428} \tag{54}$$

The same with friction factor correlation, the Nusselt number correlations of lattice-frame structure are also obtained easily, and the height is always be defined to be characteristic length. Therefore, it is possible to compare heat transfer performance between different structures with the same porosity. With further development of manufacturing technologies, more lattice-frame structures with different shapes and sizes can be obtained. Forced convection heat transfer characteristics of these different structures can therefore be more widely investigated.

5.3 Forced convection heat transfer of structured packed beds and wire-woven structures

5.3.1 Packed beds

Forced convection heat transfer in random packed beds has been widely investigated, through both experimental and numerical methods. Many correlations for predicting HTC have been developed. However, random packed beds have poor controllability and large pressure drops. Structured packed beds have therefore been more extensively investigated in recent years. This work reviews the correlations for predicting HTC of several structured packed beds.

Romkes et al. [97] investigated CSP with five different square channel-particle diameter ratios, fitting computational fluid dynamics (CFD) results using the correlation given in Eq. (55):

$$Nu = c_1 + c_2\, Re^n\, Pr^{1/3} \tag{55}$$

where c_1, c_2, and n are constant and the characteristic length is the particle diameter. These constants are different for five square channel-particle diameter ratios.

Yang et al. [145] numerically investigated a number of novel structured packed beds with different particle shapes, also comparing packed beds with non-uniform and uniform particles. They further developed interstitial Nusselt number correlations for these packed beds based on Eq. (56):

$$Nu = c_1 + c_2\, Re_{d_h}^{n}\, Pr^{1/3} \left(\frac{d_p}{d_h}\varepsilon\right)^{n} \tag{56}$$

where $d_h = 4\dfrac{\varepsilon}{1-\varepsilon}\left(\dfrac{V_p}{A_p}\right)$; $d_h = 2\left(\dfrac{3V_p}{4\pi}\right)^{1/3}$; $Re = \dfrac{ud_h}{\varepsilon\nu}$, and A_p and V_p are the particle surface and volume, respectively. The authors [142] also experimentally investigated packed beds using single blow methods, finding that numerical methods are appropriate for determining the interstitial Nusselt number. With proper selection, some structured packed beds can reduce pressure drop and improve heat transfer. The Nusselt number for such packed beds is over-predicted when using Wakao's equation [168] given in Eq. (57):

$$Nu = 2 + 1.1\, Re_{d_h}^{0.6}\, Pr^{1/3} \tag{57}$$

Wang et al. [98] developed the GSCSPB and investigated its pressure drop and heat transfer performance. It was found to have lower pressure drop and higher overall heat transfer than random packed beds and some traditional structured beds.

5.3.2 Wire-woven structure

Wire-woven structures have similar thermal performance to lattice-frame structures due to similar geometry. Some differences between these two can be attributed to the tortuous shape and thicker ligaments of lattice-frame structures [80]. Few authors have investigated the thermal performance of wire-woven structures and few correlations for these have been developed. Tian et al. [146] experimentally investigated the overall heat transfer performance of two wire-woven structures with square-shaped and diamond-shaped pores, respectively, using steady-state methods. They found that ε and surface area density have a strong influence on overall heat transfer, while direction has only a weak influence. Joo et al. [148] experimentally investigated the heat transfer performance of five-layered WBK under forced convection heat transfer and single heating. They found that the Nusselt number increased with a decrease in open area ratio, developing the WBK Nusselt number predictive correlation for two directions given in Eq. (58):

A-direction

$$Nu_H = 0.183\, Re_H^{0.8}\, Pr^{0.4} \quad 5.5\times10^3 \le Re_H \le 1.8\times10^4 \tag{58a}$$

$$Nu_{S_y} = 0.14\, Re_{S_y}^{0.68} \quad 1.8\times10^3 \le Re_H \le 3.3\times10^4 \tag{58b}$$

B-direction

$$Nu_H = 0.212\, Re_H^{0.8}\, Pr^{0.4} \quad 5.2\times10^3 \le Re_H \le 3.1\times10^4 \tag{58c}$$

where $Re_H = \dfrac{\rho u H}{\mu}$ and Pr is assumed to be 0.7. Joo et al. [8] also developed predictive correlations for three-layered WBK using the same method as previous work; the equations are given below:

A-direction

$$Nu_{D_h} = 0.3137\, Re_{D_h}^{0.785} \quad 2.0\times10^3 \le Re_H \le 2.0\times10^4 \tag{59a}$$

B-direction

$$Nu_{D_h} = 0.4824\, Re_{D_h}^{0.751} \quad 2.0\times10^3 \le Re_H \le 2.0\times10^4 \tag{59b}$$

For a given Reynolds number range, the Nusselt number of the A-direction is lower than that of the B-direction. Shen et al. [147] numerically investigated the heat transfer characteristic of single-layered WBK in the Reynolds number range of 3995 to 8710, comparing the Nusselt numbers of WBK and Kagome structures. For similar pressure drop, they found that the overall Nusselt number of Kagome is 26% to 31% higher than that of the WBK, while the Nusselt number of WBK ligaments is 42% higher than that of Kagome.

From the above review, it can be concluded that, with proper design, structured packed beds have potential for heat transfer enhancement. The heat transfer performance of structured packed bed forms should be more widely investigated. In the case of wire-woven structures, there is limited literature investigating the heat transfer performance and few predictive correlations have been developed; more research is therefore needed.

6. Application of Porous Structures to Enhance Heat Transfer

Due to their advantageous thermal properties, porous structures can be applied in many fields, such as chemical, aerospace, electronics, and energy engineering, and others. This section will introduce some applications of open-cell foam structures, lattice-frame structures, structured packed beds, and wire-woven structures.

6.1 Application of open-cell foam

Open-cell foam structures hold promise for many applications. In particular, there are many ways to use open-cell metal foams to enhance heat transfer in different situations. Many authors have explored the use of heat sinks filled with metal foam for electronic cooling [169, 170], finding that they have better heat transfer properties than the conventional heat sinks. The tube bank heat exchanger is widely used in thermal engineering. To enhance its heat transfer properties, some authors investigated wrapping the exchanger in metal

foam [171, 172]. Odabaee et al. [172] found that the heat transfer properties of a tube wrapped with metal foam are an order of magnitude higher than of an empty tube; however, the pressure drop increases. Research has also focused on optimization of heat exchanger design to enhance heat transfer with less pressure drop, for example through partially wrapped tubes [171], and wrapping with gradient metal foam [173]. Another application of metal foam in heat exchangers is using it to fill passages [174, 175]. Lu et al. [175] found that the heat transfer properties of tubes filled with metal foam were forty times higher than that of empty tubes. Partially-filled passages can therefore enhance heat transfer with smaller pressure drop [176–178]. Other novel ways to enhancing heat transfer have also been developed, such as metal foam with coating [179], metal foam heat exchangers for high temperature flow [180], and double tubes filled with metal foam [181]. In addition, with the development of 3D printing, the pore structure of open-cell foam can be designed to improve overall heat transfer performance. Some structures used to model real pore structure of open-cell foam should be considered. And then, a more accurate predictive correlation is possible to develop for the application of open-cell foam.

6.2 Application of Lattice-frame structure

Lattice-frame structures can be used in plate-fin heat exchangers for aerospace applications and power engineering, and others, due to the good load-bearing and heat transfer properties. However, there has been little investigation of the heat transfer properties of complete heat transfer devices. Yan et al. [182] used X-type structures for brake discs, investigating related heat transfer properties. X-type structure brake discs showed better heat transfer properties than radial vane brake discs. With further development of manufacturing technologies, compact heat exchangers can be obtained and their heat transfer properties should be investigated.

6.3 Application of packed beds and wire-woven structruies

Packed beds are widely used for enhancing heat transfer, for example in solar receivers, high temperature gas-cooled nuclear applications [183], and others. Structured packed beds have especially good heat transfer properties, with lower pressure drop. Compared to packed beds, wire-woven structures are more widely used for designing heat exchangers, such as wire-on-tube heat exchangers [32, 184], brake discs [167], and plate-fin exchangers.

The application of porous structures in engineering to enhance heat exchange is still limited, due to ambiguities about heat transfer properties. However, these structures could contribute to the design of heat transfer devices in future, due to their excellent structural features. More work is therefore needed to determine their heat transfer properties.

7. Conclusion

The porosity is considered as one of the most significant morphological characteristics for the performance of force convection heat transfer in the discussed light-weight porous media. For open-cell foam, the pressure drop and heat transfer coefficient are also governed by pore diameter, tortuosity and specific surface area. Note that, the specific surface area and tortuosity are determined by porosity and pore diameter. Therefore, porosity and pore diameter were most commonly taken into consideration. For lattice-frame structure, wire-woven structure and structured packed beds, the morphologic structure is crucial for the determination of porosity and property and thereby playing an important role in the heat transfer.

Currently, there is no general predicting correlation for open-cell foam structure due to the inaccurate determination of morphological characteristic, selection of characteristic length and flow laws, and difficulty in experiments. Besides, the difference in the predictions increases with an increase in velocity; especially, the gap is huge at turbulence regions with high Reynolds numbers. The general predicting correlation is more available for lattice-frame structure, wire-woven structure and structured packed beds due to the controllable structure.

Although there is substantial work on the forced heat transfer in porous structure, more researches should be carried in the following aspect: more accurate determination of the morphological characteristics and selection of a more general characteristic length; development of more accurate prediction correlations at turbulence regions with high Reynolds numbers; further controlled organization of the structure of lattice-frame, structured packed beds, and wire-woven structures.

Acknowledgement

This study was supported by the National Science and Technology Major Project (2017-III-0005-0029), the National Natural Science Foundation of China (Grant Nos. 51806027, U19B2005) and the National Key R&D Program of China (Grant No. 2018YFC0310006).

References

[1] Albanakis C., Yakinthos K., Kritikos K., Missirlis D., The effect of heat transfer on the pressure drop through a heat

exchanger for aero engine applications. Applied Thermal Engineering, 2009, 29(4): 634–644.

[2] Wen J., Huang H.R., Li H.W., Xu G.Q., Fu, Y.C., Thermal and hydraulic performance of a compact plate finned tube air-fuel heat exchanger for aero-engine. Applied Thermal Engineering, 2017, 126: 920–928.

[3] Fu Y.X., He Z.X., Mo D.C., Lu S.S., Thermal conductivity enhancement with different fillers for epoxy resin adhesives. Applied Thermal Engineering, 2014, 66(1–2): 493–498.

[4] Kim I.H., No H.C., Thermal hydraulic performance analysis of a printed circuit heat exchanger using a helium-water test loop and numerical simulations. Applied Thermal Engineering, 2011, 31(17–18): 4064–4073.

[5] Aquaro D., Pieve M., High temperature heat exchangers for power plants: Performance of advanced metallic recuperators. Applied Thermal Engineering, 2007, 27(2–3): 389–400.

[6] Zhang L.X., Yang L., Wang J.Q., Zhao J.F., Enhanced CH_4 recovery and CO_2 storage via thermal stimulation in the CH_4/CO_2 replacement of methane hydrate. Chemical Engineering Journal, 2017, 308: 40–49.

[7] Fuller A.J., Kim T., Hodson H.P., Lu T.J., Measurement and interpretation of the heat transfer coefficients of metal foams. Proceedings of the Institution of Mechanical Engineers Part C: Journal of Mechanical Engineering Science, 2005, 219(2): 183–191.

[8] Joo J.H., Kang K.J., Kim T., Lu T.J., Forced convective heat transfer in all metallic wire-woven bulk Kagome sandwich panels. International Journal of Heat and Mass Transfer, 2011, 54(25–26): 5658–5662.

[9] Kim T., Hodson H.P., Lu T.J., Fluid-flow and endwall heat-transfer characteristics of an ultralight lattice-frame material. International Journal of Heat and Mass Transfer, 2004, 47(6–7): 1129–1140.

[10] Zhao C.Y., Kim T., Lu T.J., Hodson H.P., Thermal transport in high porosity cellular metal foams. Journal of Thermophysics and Heat Transfer, 2004, 18(3): 309–317.

[11] Zheng K.C., Wen Z., Wang Z.S., Lou G.F., et al., Review on forced convection heat transfer in porous media. Acta Physica Sinica, 2012, 61(1): 014401-1-11.

[12] Mandi R.A., Mohammed H.A., Munisamy K.M., Saeid N.H., Review of convection heat transfer and fluid flow in porous media with nanofluid. Renewable & Sustainable Energy Reviews, 2015, 41: 715–734.

[13] Han X.H., Wang Q., Park Y.G., T'Joen C., et al., A review of metal foam and metal matrix composites for heat exchangers and heat sinks. Heat Transfer Engineering, 2012, 33(12): 991–1009.

[14] Mancin S., Diani A., Doretti L., Rossetto L., R134a and R1234ze(E) liquid and flow boiling heat transfer in a high porosity copper foam. International Journal of Heat and Mass Transfer, 2014, 74: 77–87.

[15] Abadi G.B., Moon C., Kim K.C., Experimental study on single-phase heat transfer and pressure drop of refrigerants in a plate heat exchanger with metal-foam-filled channels. Applied Thermal Engineering, 2016, 102: 423–431.

[16] Kim D.Y., Kim K.C., An experimental study on the thermal and hydraulic characteristics of open-cell nickel and copper foams for compact heat exchangers. International Journal of Heat and Mass Transfer, 2019, 130: 162–174.

[17] Kim T., Zhao C.Y., Lu T.J., Hodson H.P., Convective heat dissipation with lattice-frame materials. Mech Mater, 2004, 36(8): 767–780.

[18] Mancin S., Zilio C., Rossetto L., Cavallini A., Heat transfer performance of Aluminum foams. Journal of Heat Transfer-transactions of Asme, 2011, 133(6): 060904-1-9.

[19] Mancin S., Zilio C., Cavallini A., Rossetto L., Heat transfer during air flow in aluminum foams. International Journal of Heat and Mass Transfer, 2010, 53(21–22): 4976–4984.

[20] Mancin S., Zilio C., Cavallini A., Rossetto L., Pressure drop during air flow in aluminum foams. International Journal of Heat and Mass Transfer, 2010, 53(15–16): 3121–3130.

[21] Mancin S., Zilio C., Diani A., Rossetto L., Air forced convection through metal foams: Experimental results and modeling. International Journal of Heat and Mass Transfer, 2013, 62: 112–123.

[22] Dietrich B., Heat transfer coefficients for solid ceramic sponges - Experimental results and correlation. International Journal of Heat and Mass Transfer, 2013, 61: 627–637.

[23] Dietrich B., Schabel W., Kind M., Martin H., Pressure drop measurements of ceramic sponges-Determining the hydraulic diameter. Chemical Engineering Science, 2009, 64(16): 3633–3640.

[24] Wallenstein M., Kind M., Dietrich B., Radial two-phase thermal conductivity and wall heat transfer coefficient of ceramic sponges - Experimental results and correlation. International Journal of Heat and Mass Transfer, 2014, 79: 486–495.

[25] Moreira E.A., Innocentini M.D. M., Coury J.R., Permeability of ceramic foams to compressible and incompressible flow. Journal of the European Ceramic Society, 2004, 24(10–11): 3209–3218.

[26] Moreira E.A., Coury J.R., The influence of structural parameters on the permeability of ceramic foams. Brazilian Journal of Chemical Engineering, 2004, 21(1): 23–33.

[27] Giani L., Groppi G., Tronconi E., Mass-transfer characterization of metallic foams as supports for

structured catalysts. Industrial & Engineering Chemistry Research, 2005, 44(14): 4993–5002.

[28] Xia X.L., Chen X., Sun C., Li Z.H., Liu B., Experiment on the convective heat transfer from airflow to skeleton in open-cell porous foams. International Journal of Heat and Mass Transfer, 2017, 106: 83–90.

[29] Lacroix M., Nguyen P., Schweich D., Huu C.P., et al., Pressure drop measurements and modeling on SiC foams. Chemical Engineering Science, 2007, 62(12): 3259–3267.

[30] Dixit T., Ghosh I., An experimental study on open cell metal foam as extended heat transfer surface. Experimental Thermal and Fluid Science, 2016, 77: 28–37.

[31] Yan H.B., Yang X.H., Lu T.J., Xie G.N., Convective heat transfer in a lightweight multifunctional sandwich panel with X-type metallic lattice core. Applied Thermal Engineering, 2017, 127: 1293–1304.

[32] Kurian R., Balaji C., Venkateshan S.P., Experimental investigation of near compact wire mesh heat exchangers. Applied Thermal Engineering, 2016, 108: 1158–1167.

[33] Nawaz K., Bock J., Jacobi A.M., Thermal-hydraulic performance of metal foam heat exchangers under dry operating conditions. Applied Thermal Engineering, 2017, 119: 222–232.

[34] T'Joen C., De Jaeger P., Huisseune H., Van Herzeele S., et al., Thermo-hydraulic study of a single row heat exchanger consisting of metal foam covered round tubes. International Journal of Heat and Mass Transfer, 2010, 53(15–16): 3262–3274.

[35] Chen K., Guo L.J., Xie X.D., Liu W.Z., Experimental investigation on enhanced thermal performance of staggered tube bundles wrapped with metallic foam. International Journal of Heat and Mass Transfer, 2018, 122: 459–468.

[36] Madani B., Topin F., Rigollet F., Tadrist L., Flow laws in metallic foams: Experimental determination of inertial and viscous contributions. Journal of Porous Media, 2007, 10(1): 51–70.

[37] Garrido G.I., Patcas F.C., Lang S., Kraushaar-Czarnetzki B., Mass transfer and pressure drop in ceramic foams: A description for different pore sizes and porosities. Chemical Engineering Science, 2008, 63(21): 5202–5217.

[38] Son K.N., Weibel J.A., Kumaresan V., Garimella S.V., Design of multifunctional lattice-frame materials for compact heat exchangers. International Journal of Heat and Mass Transfer, 2017, 115: 619–629.

[39] Dukhan N., Minjeur C.A., A two-permeability approach for assessing flow properties in metal foam. Journal of Porous Materials, 2011, 18(4): 417–424.

[40] Banhart J., Manufacture, characterisation and application of cellular metals and metal foams. Progress in Materials Science, 2001, 46(6): 559–632.

[41] Deng X., Wang J., Shuang D., Cao Y., Li F.L., Fabricating porous ceramic through direct foaming, three-dimensional printing and molten salt method. Materials Review, 2015, 29(5): 109–116.

[42] Li J., Yang Q.M., Zhitornirsky I., Nickel foam-based manganese dioxide-carbon nanotube composite electrodes for electrochemical supercapacitors. Journal of Power Sources, 2008, 185(2): 1569–1574.

[43] Harte A.M., Fleck N.A., Ashby M.F., Fatigue failure of an open cell and a closed cell aluminium alloy foam. Acta Materialia, 1999, 47(8): 2511–2524.

[44] Bram M., Stiller C., Buchkremer H.P., Stover D., Baur H., High-porosity titanium, stainless steel, and superalloy parts. Advanced Engineering Materials, 2000, 2(4): 196–199.

[45] Liu P.S., Chen G.F., General introduction to porous materials. 2014, pp. 1–20.

[46] Pal L., Joyce M.K., Fleming P.D., A simple method for calculation of the permeability coefficient of porous media. Tappi Journal, 2006, 5(9): 10–16.

[47] Schwartzwalder A.E., Sommer A.V., Method of making porous ceramic articles. U.S Patent office, 1963, pp. 90–94.

[48] Inayat A., Klumpp M., Lammermann M., Freund H., Schwieger W., Development of a new pressure drop correlation for open-cell foams based completely on theoretical grounds: Taking into account strut shape and geometric tortuosity. Chemical Engineering Journal, 2016, 287: 704–719.

[49] Grosse J., Dietrich B., Martin H., Kind M., et al., Volume image analysis of ceramic sponges. Chemical Engineering & Technology, 2008, 31(2): 307–314.

[50] Inayat A., Freund H., Zeiser T., Schwieger W., Determining the specific surface area of ceramic foams: The tetrakaidecahedra model revisited. Chemical Engineering Science, 2011, 66(6): 1179–1188.

[51] Boomsma K., Poulikakos D., Ventikos Y., Simulations of flow through open cell metal foams using an idealized periodic cell structure. International Journal of Heat and Fluid Flow, 2003, 24(6): 825–834.

[52] Xu W.G., Zhang H.T., Yang Z.M., Zhang J.S., Numerical investigation on the flow characteristics and permeability of three-dimensional reticulated foam materials. Chemical Engineering Journal, 2008, 140(1–3): 562–569.

[53] Kumar P., Topin F., Micro-structural impact of different strut shapes and porosity on hydraulic properties of Kelvin-like metal foams. Transport in Porous Media, 2014, 105(1): 57–81.

[54] Kumar P., Topin F., Investigation of fluid flow properties in open cell foams: Darcy and weak inertia regimes. Chemical Engineering Science, 2014, 116: 793–805.

[55] Bonnet J.P., Topin F., Tadrist L., Flow laws in metal

foams: Compressibility and pore size effects. Transport in Porous Media, 2008, 73(2): 233–254.

[56] Boomsma K., Poulikakos D., The effects of compression and pore size variations on the liquid flow characteristics in metal foams. Journal of Fluids Engineering-Transactions of the Asme, 2002, 124(1): 263–272.

[57] Lage J.L., Antohe B.V., Darcy's experiments and the deviation to nonlinear flow regime. Journal of Fluids Engineering-Transactions of the Asme, 2000, 122(3): 619–625.

[58] Murilo D.M. Innocentini V.R.S., Alvaro M., Prediction of ceramic foams permeability using Ergun's equation. Materials Research, 1999, 2(4): 283–289.

[59] Richardson J.T., Peng Y., Remue D., Properties of ceramic foam catalyst supports: pressure drop. Applied Catalysis a-General, 2000, 204(1): 19–32.

[60] Dukhan N., Patel P., Equivalent particle diameter and length scale for pressure drop in porous metals. Experimental Thermal and Fluid Science, 2008, 32(5): 1059–1067.

[61] Ahmed J., Pham-Huu C., Edouard D., A predictive model based on tortuosity for pressure drop estimation in "slim" and "fat" foams. Chemical Engineering Science, 2011, 66(20): 4771–4779.

[62] Huu T.T., Lacroix M., Huu C.P., Schweich D., Edouard D., Towards a more realistic modeling of solid foam: Use of the pentagonal dodecahedron geometry. Chemical Engineering Science, 2009, 64(24): 5131–5142.

[63] Diao K.K., Zhang L.P., Zhao Y.Y., Measurement of tortuosity of porous Cu using a diffusion diaphragm cell. Measurement, 2017, 110: 335–338.

[64] Le L.H., Zhang C., Ta D., Lou E., Measurement of tortuosity in aluminum foams using airborne ultrasound. Ultrasonics, 2010, 50(1): 1–5.

[65] Haussener S., Coray P., Lipinski W., Wyss P., Steinfeld A., Tomography-based heat and mass transfer characterization of reticulate porous ceramics for high-temperature processing. Journal of Heat Transfer-Transactions of the Asme, 2010, 132(2): 023305-1-9.

[66] Bodla K.K., Murthy J.Y., Garimella S.V., Microtomography-based simulation of transport through open-cell metal foams. Numerical Heat Transfer Part a-Applications, 2010, 58(7): 527–544.

[67] Habisreuther P., Djordjevic N., Zarzalis N., Statistical distribution of residence time and tortuosity of flow through open-cell foams. Chemical Engineering Science, 2009, 64(23): 4943–4954.

[68] Letellier M., Fierro V., Pizzi A., Celzard A., Tortuosity studies of cellular vitreous carbon foams. Carbon, 2014, 80: 193–202.

[69] Duplessis P., Montillet A., Comiti J., Legrand J., Pressure-drop prediction for flow-through high-porosity metallic foams. Chemical Engineering Science, 1994, 49(21): 3545–3553.

[70] Bhattacharya A., Calmidi V.V., Mahajan R.L., Thermophysical properties of high porosity metal foams. International Journal of Heat and Mass Transfer, 2002, 45(5): 1017–1031.

[71] Vicente J., Topin F., Daurelle J.V., Open celled material structural properties measurement: From morphology to transport properties. Materials Transactions, 2006, 47(9): 2195–2202.

[72] Bianchi E., Heidig T., Visconti C.G., Groppi G., et al., An appraisal of the heat transfer properties of metallic open-cell foams for strongly exo-/endo-thermic catalytic processes in tubular reactors. Chemical Engineering Journal, 2012, 198: 512–528.

[73] Diao K.K., Xiao Z., Zhao Y.Y., Specific surface areas of porous Cu manufactured by lost carbonate sintering: Measurements by quantitative stereology and cyclic voltammetry. Materials Chemistry and Physics, 2015, 162: 571–579.

[74] Liu J.F., Wu W.T., Chiu W.C., Hsieh W.H., Measurement and correlation of friction characteristic of flow through foam matrixes. Experimental Thermal and Fluid Science, 2006, 30(4): 329–336.

[75] Gibson L.J., Ashby M.F., Cellular solids, structures and properties. Pergamon press Oxford, 1988.

[76] Buciuman F.C., Kraushaar-Czarnetzki B., Ceramic foam monoliths as catalyst carriers. 1. Adjustment and description of the morphology. Industrial & Engineering Chemical Research, 2003, 42(9): 1863–1869.

[77] Kumar P., Topin F., The geometric and thermohydraulic characterization of ceramic foams: An analytical approach. Acta Materialia, 2014, 75: 273–286.

[78] Grosse J., Dietrich B., Garrido G.I., Habisreuther, P., et al., Morphological characterization of ceramic sponges for applications in chemical engineering. Industrial & Engineering Chemistry Research, 2009, 48(23): 10395–10401.

[79] Queheillalt D.T., Wadley H.N.G., Cellular metal lattices with hollow trusses. Acta Materialia, 2005, 53(2): 303–313.

[80] Kang K.J., Wire-woven cellular metals: The present and future. Progress in Materials Science, 2015, 69: 213–307.

[81] Deshpande V.S., Fleck N.A., Ashby M.F., Effective properties of the octet-truss lattice material. Journal of the Mechanics Physics of Solids, 2001, 49(8): 1747–1769.

[82] Wadley H.N.G., Fleck N.A., Evans A.G., Fabrication and structural performance of periodic cellular metal sandwich structures. Composites Science and Technology, 2003, 63(16): 2331–2343.

[83] Yan H.B., Zhang Q.C., Lu T.J., Kim T., A lightweight X-type metallic lattice in single-phase forced convection.

International Journal of Heat and Mass Transfer, 2015, 83: 273–283.

[84] St-Pierre L., Fleck N.A., Deshpande V.S., The predicted compressive strength of a pyramidal lattice made from case hardened steel tubes. International Journal of Solids and Structure, 2014, 51(1): 41–52.

[85] Wei K., He R.J., Cheng X.M., Pei Y.M.., et al., Fabrication and heat transfer characteristics of C/SiC pyramidal core lattice sandwich panel. Applied Thermal Engineering, 2015, 81: 10–17.

[86] Xiong J., Ma L., Pan S., Wu L., et al., Shear and bending performance of carbon fiber composite sandwich panels with pyramidal truss cores. Acta Materialia, 2012, 60(4): 1455–1466.

[87] Liu J.Y., Zhu X., Zhou Z.G., Wu L.Z., Ma L., Effects of thermal exposure on mechanical behavior of carbon fiber composite pyramidal truss core sandwich panel. Composites Part B-Engineering, 2014, 60: 82–90.

[88] Wu Q.Q., Ma L., Wu L.Z., Xiong J., A novel strengthening method for carbon fiber composite lattice truss structures. Compos Structure, 2016, 153: 585–592.

[89] Antwerpen W., Toit C.G., Rousseau P.G., A review of correlations to model the packing structure and effective thermal conductivity in packed beds of mono-sized spherical particles. Nuclear Engineering and Design, 2010, 240(7): 1803–1818.

[90] Haughey D.P., Beveridge G.S., Structural properties of packed beds - a review. Canadian Journal of Chemical Engineering, 1969, 47(2): 130.

[91] Roblee L. H.S., Baird R.M., Tierney J.W., Radial porosity variations in packed beds. Aiche Journal, 1958, 4(4): 460–464.

[92] Carman C.P., Fluid flow through Granular beds. Transactions of the Institution of Chemical Engineers, 1937, 15: 150.

[93] Leva M., Grummer M., Pressure drop through packed tubes 3. prediction of voids in packed tubes. Chemical Engineering Progress, 1947, 43(12): 713–718.

[94] Rutgers R., Packing of spheres. Nature, 1962, 193(4814): 465–466.

[95] Scott G.D., Packing of equal spheres. Nature, 1960, 188(4754): 908–909.

[96] Foumeny E.A., Moallemi H.A., Mcgreavy C., Castro J.A.A., Elucidation of mean voidage in packed-beds. Canadian Journal of Chemical Engineering, 1991, 69(4): 1010–1015.

[97] Romkes S.J.P., Dautzenberg E., van den Bleek C.M., Calis H.P.A., CFD modelling and experimental validation of particle-to-fluid mass and heat transfer in a packed bed at very low channel to particle diameter ratio. Chemical Engineering Journal, 2003, 96(1–3): 3–13.

[98] Wang J.Y., Yang J., Cheng Z.L., Liu Y., et al., Experimental and numerical study on pressure drop and heat transfer performance of grille-sphere composite structured packed bed. Applied Energy, 2018, 227: 719–730.

[99] Wallach J.C, Gibson L.J., Truss core sandwich panels and methods for making same. US Patent, November 21, 2002, no. US6644535B2.

[100] Choi K.S. Kang K., Assembly of coil springs and sandwich panel using the same. Korea patent, March 20, 2007, No. 10-0700212.

[101] Lim J.H., Kang K.J., Wire formed cellular metals. Materials Transactions, 2006, 47(9): 2154–2160.

[102] Lim J.H., Kang K.J., Mechanical behavior of sandwich panels with tetrahedral and Kagome truss cores fabricated from wires. International Journal of Solids Structures, 2006, 43(17): 5228–5246.

[103] Kim H., Kang K.J., Joo J.H., A zigzag-formed truss core and its mechanical performances. Journal of Sandwich Structure & Materials, 2010, 12(3): 351–368.

[104] Kang K.J., Lee C.J., Lee D.S., Lee B.C., A light weight sandwich panel with a core constructed of wires and the manufacturing method of the same. Korea patent, October 8, 2007, no. 10-0767186.

[105] Sennewald C.A.O., Böhm R., Cherif C.H., Hoffmann G., Gruhl A., Textile based metal sandwiches and metal-matrix-composites reinforced with 3D wire structures. Part I: development and realisation of cellular 3D wire structures. Proceedings of 15th European conference on composite materials, Venice, Italia, 2012.

[106] Kaina S., Kieback B., Hufenbach W., Weck D., Gruhl A., Thieme M., Böhm R., Cherif C., Sennewald C., Cellular metal for lightweight design based on textile wire structures. Proceedings of CELLMAT2012, Dresden, Germany, 2012.

[107] Sypeck D.J., Wadley H.N.G., Multifunctional microtruss laminates: Textile synthesis and properties. Journal of Materials Research, 2001, 16(3): 890–897.

[108] Lee Y.H., Lee B., Jeon I., Kang K.J., Wire-woven bulk Kagome (WBK) truss cores. Acta Materials, 2007, 55: 6084–6094.

[109] Kieselstein E., Weinrich T., Adam F., Weck D., Gottwald R., Studnitzky T., Cellular metals based on 3D-wire structures. 6th International conference on porous metals and metallic foams, September 1–4, 2009.

[110] Lee M.G., Ko G.D., Song J., Kang K.J., Compressive characteristics of a wire-woven cellular metal. Materials Science and Engineering a-Structural Materials Properties Microstructure and Processing, 2012, 539: 185–193.

[111] Lee M.G., Kang K.J., Feasibility of a wire-woven metal for application as a sandwich core. International Journal of Mechanical Sciences, 2014, 80: 81–92.

[112] Lee M.G., Lee K.W., Hur H.K., Kang K.J., Mechanical behavior of a wire-woven metal under compression.

Composite Structures, 2013, 95: 264–277.

[113] Sharp K.M.D., Brown J., Metallic cellular materials produced by 3D weaving. 8th International Conference on Porous Metals and Metallic Foams, 2014.

[114] Guo Z.Y., Xiong D.X., Yang C., Chen M., Li Z.X., Continuous liquid-vapor phase transition in microspace. International Journal of Thermal Sciences, 2000, 39(4): 481–489.

[115] Chen G.M., Tso C.P., Hung Y.M., Field synergy principle analysis on fully developed forced convection in porous medium with uniform heat generation. International Communications in Heat and Mass Transfer, 2011, 38(9): 1247–1252.

[116] Peng Q.G., E, J.Q., Chen J.W., Zuo W., et al., Investigation on the effects of wall thickness and porous media on the thermal performance of a non-premixed hydrogen fueled cylindrical micro combustor. Energy Conversion and Management, 2018, 155: 276–286.

[117] Wang G.H., Wang D.B., Deng J., Lyu Y.M., et al., Experimental and numerical study on the heat transfer and flow characteristics in shell side of helically coiled tube heat exchanger based on multi-objective optimization. International Journal of Heat and Mass Transfer, 2019, 137: 349–364.

[118] Bagci O., Dukhan N., Experimental hydrodynamics of high-porosity metal foam: Effect of pore density. International Journal of Heat and Mass Transfer, 2016, 103: 879–885.

[119] Dukhan N., Bagci O., Ozdemir M., Metal foam hydrodynamics: Flow regimes from pre-Darcy to turbulent. International Journal of Heat and Mass Transfer, 2014, 77: 114–123.

[120] Hwang J.J., Hwang G.J., Yeh R.H., Chao C.H., Measurement of interstitial convective heat transfer and frictional drag for flow across metal foams. Journal of Fluids Engineering-Transactions of the ASME, 2002, 124(1): 120–129.

[121] Dukhan N., Patel K., Effect of sample's length on flow properties of open-cell metal foam and pressure-drop correlations. Journal of Porous Materials, 2011, 18(6): 655–665.

[122] Vafai K., Tien C.L., Boundary and inertia effects on convective mass-transfer in porous-media. International Journal of Heat and Mass Transfer, 1982, 25(8): 1183–1190.

[123] Kumar P., Topin E., State-of-the-art of pressure drop in open-Cell porous foams: Review of experiments and correlations. Journal of Fluids Engineering-Transactions of the Asme, 2017, 139(11): 111401-1-13.

[124] Ergun S., Orning A.A., Fluid flow through randomly packed columns and fluidized beds. Industrial & Engineering Chemistry, 1949, 41(6): 1179–1184.

[125] Twigg M.V., Richardson J.T., Fundamentals and applications of structured ceramic foam catalysts. Industrial & Engineering Chemistry Research, 2007, 46(12): 4166–4177.

[126] Dietrich B., Pressure drop correlation for ceramic and metal sponges. Chemical Engineering Science, 2012, 74: 192–199.

[127] Edouard D., Lacroix M., Huu C.P., Luck F., Pressure drop modeling on SOLID foam: State-of-the art correlation. Chemical Engineering Journal, 2008, 144(2): 299–311.

[128] Kumar P., Topin F., Influence of morphology on flow law characteristics in open-cell foams: an overview of usual approaches and correlations. Journal of Fluids Engineering-Transactions of the ASME, 2017, 139(7): 071301-1-12.

[129] Topin F., Bonnet J.P., Madani B., Tadrist L., Experimental analysis of multiphase flow in metallic foam: Flow laws, heat transfer and convective boiling. Advanced Engineering Materials, 2006, 8(9): 890–899.

[130] Dukhan N., Correlations for the pressure drop for flow through metal foam. Experiments in Fluids, 2006, 41(4): 665–672.

[131] Dukhan N., Picon-Feliciano R., Alvarez-Hernandez A.R., Air flow through compressed and uncompressed aluminum foam: Measurements and correlations. Journal of Fluids Engineering-Transactions of the ASME, 2006, 128(5): 1004–1012.

[132] Tadrist, L., Miscevic, M., Rahli, O., Topin, F., About the use of fibrous materials in compact heat exchangers. Experimental Thermal and Fluid Science, 2004, 28(2–3): 193–199.

[133] Khayargoli P., Loya V., Lefebvre P.L., Medraj M., The impact of microstructure on the permeability of metal foams. CSME 2004, Forum, 2004, pp. 220–228.

[134] Wu Z.Y., Caliot C., Bai F.W., Flamant G., et al., Experimental and numerical studies of the pressure drop in ceramic foams for volumetric solar receiver applications. Applied Energy, 2010, 87(2): 504–513.

[135] Inayat A., Schwerdtfeger J., Freund H., Korner C., et al., Periodic open-cell foams: Pressure drop measurements and modeling of an ideal tetrakaidecahedra packing. Chemical Engineering Science, 2011, 66(12): 2758–2763.

[136] Leong K.C., Jin L.W., Characteristics of oscillating flow through a channel filled with open-cell metal foam. International Journal of Heat and Fluid Flow, 2006, 27(1): 144–153.

[137] Kim T., Hodson H.P., Lu T.J., Contribution of vortex structures and flow separation to local and overall pressure and heat transfer characteristics in an ultralightweight lattice material. International Journal of Heat and Mass Transfer, 2005, 48(19–20): 4243–4264.

[138] Kim T., Hodson H.P., Lu T.J., Pressure loss and heat transfer mechanisms in a lattice-frame structured heat exchanger. Proceedings of the Institution of Mechanical

Engineers Part C-journal of Mechanical engineering science, 2004, 218(11): 1321–1336.

[139] Swaminathan G.K., Karthik K.B., Justin A.W., Suresh V.G., Numerical investigation of fluid flow and heat transfer in periodic porous lattice-frame materials. IHTC16, 2014, pp. 6651–6665.
DOI: 10.1615/IHTC15.pmd.008706.

[140] Hoffmann F., Heat transfer performance and pressure drop of Kagome core metal truss panels. Master thesis, University of Cambridge, Cambridge, UK, 2002.

[141] Erdim E., Akgiray O., Demir I., A revisit of pressure drop-flow rate correlations for packed beds of spheres. Powder Technology, 2015, 283: 488–504.

[142] Yang J., Wang J., Bu S.S., Zeng M., et al., Experimental analysis of forced convective heat transfer in novel structured packed beds of particles. Chemical Engineering Sciences, 2012, 71: 126–137.

[143] Calis H.P.A., Nijenhuis J., Paikert B.C., Dautzenberg F.M., van den Bleek C.M., CFD modelling and experimental validation of pressure drop and flow profile in a novel structured catalytic reactor packing. Chemical Engineering Sciences, 2001, 56(4): 1713–1720.

[144] Susskind H., Becker W., Pressure drop in geometrically ordered packed beds of spheres. AIChE Journal, 1967, 13(6): 1155–1159.

[145] Yang J., Wang Q.W., Zeng M., Nakayama A., Computational study of forced convective heat transfer in structured packed beds with spherical or ellipsoidal particles. Chemical Engineering Sciences, 2010, 65(2): 726–738.

[146] Tian J., Kim, T., Lu T.J., Hodson H.P., et al., The effects of topology upon fluid-flow and heat-transfer within cellular copper structures. International Journal of Heat and Mass Transfer, 2004, 47(14–16): 3171–3186.

[147] Shen B.B., Yan H.B., Xue H.Q., Xie G.N., The effects of geometrical topology on fluid flow and thermal performance in Kagome cored sandwich panels. Applied Thermal Engineering, 2018, 142: 79–88.

[148] Joo J.H., Kang B.S., Kang K.J., Experimental studies on friction factor and heat transfer characteristics through wire-woven bulk Kagome structure. Experimental Heat Transfer, 2009, 22(2): 99–116.

[149] Vafai K., Handbook of porous media. Third Edition, CRC Press, 2015.

[150] Zhao C.Y., Review on thermal transport in high porosity cellular metal foams with open cells. International Journal of Heat and Mass Transfer, 2012, 55(13–14): 3618–3632.

[151] Nakayama A., Ando K., Yang C., Sano Y., et al., A study on interstitial heat transfer in consolidated and unconsolidated porous media. Heat Mass Transfer, 2009, 45(11): 1365–1372.

[152] Wu Z.Y., Caliot C., Flamant G., Wang Z.F., Numerical simulation of convective heat transfer between air flow and ceramic foams to optimise volumetric solar air receiver performances. International Journal of Heat and Mass Transfer, 2011, 54(7–8): 1527–1537.

[153] Younis L.B., Viskanta R., Experimental-determination of the volumetric heat-transfer coefficient between stream of air and ceramic foam. International Journal of Heat and Mass Transfer, 1993, 36(6): 1425–1434.

[154] Lu T.J., Stone H.A., Ashby M.F., Heat transfer in open-cell metal foams. Acta Material, 1998, 46(10): 3619–3635.

[155] Wu D.X., Huang C.L., Thermal conductivity model of open-cell foam suitable for wide span of porosities. International Journal of Heat and Mass Transfer, 2019, 130: 1075–1086.

[156] Bai M., Chung J.N., Analytical and numerical prediction of heat transfer and pressure drop in open-cell metal foams. International Journal Thermal Science, 2011, 50(6): 869–880.

[157] Fu X., Viskanta R., Gore J.P., Measurement and correlation of volumetric heat transfer coefficients of cellular ceramics. Experimental Thermal Fluid Science, 1998, 17(4): 285–293.

[158] Peng Y., Richardson J.T., Properties of ceramic foam catalyst supports: one-dimensional and two-dimensional heat transfer correlations. Applied Catalysis a-General, 2004, 266(2): 235–244.

[159] Giani L., Groppi G., Tronconi E., Heat transfer characterization of metallic foams. Industrial & Engineering Chemistry Research, 2005, 44(24): 9078–9085.

[160] Calmidi V.V., Mahajan R.L., Forced convection in high porosity metal foams. Journal of Heat Transfer-Transactions of the ASME, 2000, 122(3): 557–565.

[161] Ando K., Hirai H., Sano Y., An accurate experimental determination of interstitial heat transfer coefficients of ceramic foams using the single blow method. The Open Transport Phenomena Journal, 2013, 5(1): 7–12.

[162] Dukhan N., Bagci O., Ozdemir M., Thermal development in open-cell metal foam: An experiment with constant wall heat flux. International Journal of Heat and Mass Transfer, 2015, 85: 852–859.

[163] Kamiuto K., Yee S.S., Heat transfer correlations for open-cellular porous materials. International Communication in Heat and Mass Transfer, 2005, 32(7): 947–953.

[164] Ichimiya K., A new method for evaluation of heat transfer between solid material and fluid in a porous medium. Journal of Heat Transfer-Transactions of the ASME, 1999, 121(4): 978–983.

[165] Zhang X.Q., Jin X., Xie G.N., Yan H.B., Thermo-fluidic comparison between sandwich panels with tetrahedral

lattice cores fabricated by casting and metal sheet folding. Energies, 2017, 10(7): 1–17.

[166] Jin X., Shen B.B., Yan H.B., Sunden B., Xie G.N., Comparative evaluations of thermofluidic characteristics of sandwich panels with X-lattice and Pyramidal-lattice cores. International Journal of Heat and Mass Transfer, 2018, 127: 268–282.

[167] Yan H.B., Mew T., Lee M.G., Kang K.J., et al., Thermofluidic characteristics of a porous ventilated brake disk. Journal of Heat Transfer-Transactions of the ASME, 2015, 137(2): 022601-1-11.

[168] Noriaki W., Seiichir D.K., Heat and mass transfer in packed beds. Gordon and Breach, New York, 1982.

[169] Gong L., Li Y.T., Bai Z., Xu M.H., Thermal performance of micro-channel heat sink with metallic porous/solid compound fin design. Applied Thermal Engineering, 2018, 137: 288–295.

[170] Leong K.C., Li H.Y., Jin L. W., Chai J.C., Numerical and experimental study of forced convection in graphite foams of different configurations. Applied Thermal Engineering, 2010, 30(5): 520–532.

[171] Alvandifar N., Saffar-Avval M., Amani E., Partially metal foam wrapped tube bundle as a novel generation of air cooled heat exchangers. International Journal of Heat and Mass Transfer, 2018, 118: 171–181.

[172] Odabaee M., Hooman K., Application of metal foams in air-cooled condensers for geothermal power plants: An optimization study. International Communication in Heat and Mass Transfer, 2011, 38(7): 838–843.

[173] Xu Z.G., Qin J., Zhou X., Xu H.J., Forced convective heat transfer of tubes sintered with partially-filled gradient metal foams (GMFs) considering local thermal non-equilibrium effect. Applied Thermal Engineering, 2018, 137: 101–111.

[174] Kurtbas I., Celik N., Dincer I., Exergy transfer in a porous rectangular channel. Energy, 2010, 35(1): 451–460.

[175] Lu W., Zhao C.Y., Tassou S.A., Thermal analysis on metal-foam filled heat exchangers. Part I: Metal-foam filled pipes. International Journal of Heat and Mass Transfer, 2006, 49(15–16): 2751–2761.

[176] Li Y.Z., Wang S.X., Zhao Y.L., Experimental study on heat transfer enhancement of gas tube partially filled with metal foam. Experimental Thermal Fluid Science, 2018, 97: 408–416.

[177] Nimvari M.E., Jouybari N.F., Investigation of turbulence effects within porous layer on the thermal performance of a partially filled pipe. International Journal Thermal Science, 2017, 118: 374–385.

[178] Yang C., Nakayama A., Liu W., Heat transfer performance assessment for forced convection in a tube partially filled with a porous medium. International Journal Thermal Science, 2012, 54: 98–108.

[179] Lai Z.C., Hu H.T., Ding G.L., Effect of porosity on heat transfer and pressure drop characteristics of wet air in hydrophobic metal foam under dehumidifying conditions. Experimental Thermal Fluid Science, 2018, 96: 90–100.

[180] Hafeez P., Chandra S., Mostaghimi J., Heat transfer during high temperature gas flow through metal foam heat exchangers. Journal of Heat Transfer-Transactions of the Asme, 2017, 139(12): 121801-1-11.

[181] Jamarani A., Maerefat M., Jouybari N.F., Nimvari M.E., Thermal performance evaluation of a double-tube heat exchanger partially filled with porous media under turbulent flow regime. Transport in Porous Media, 2017, 120(3): 449–471.

[182] Yan H.B., Zhang Q.C., Lu T.J., An X-type lattice cored ventilated brake disc with enhanced cooling performance. International Journal of Heat and Mass Transfer, 2015, 80: 458–468.

[183] Abdulmohsin R.S., Al-Dahhan M.H., Characteristics of convective heat transport in a packed pebble-bed reactor. Nuclear Engineering and Design, 2015, 284: 143–152.

[184] Nuntaphan A., Vithayasai S., Vorayos N., Vorayos N., Kiatsiriroat T., Use of oscillating heat pipe technique as extended surface in wire-on-tube heat exchanger for heat transfer enhancement. International Communication in Heat and Mass Transfer, 2010, 37(3): 287–292.